LOX-1 is expressed not only in vascular endothelial cells but also in monocyte-derived macrophages, vascular smooth muscle cells, and chondrocytes (Moriwaki et al. 1998a; Yoshida et al. 1998; Draude et al. 1999; Aoyama et al. 2000; Nakagawa et al. 2002). Northern blot analysis of human tissues detected LOX-1 mRNA in vascular-rich organs such as placenta, lung, brain, and liver (Sawamura et al. 1997). Among these tissues, the placenta had the highest expression of LOX-1 mRNA (Sawamura et al. 1997), which indicated a crucial role of LOX-1 in placental function. It is suggested that LOX-1 might be involved in trophoblast invasion in early pregnancy (Pavan et al. 2004; Fournier et al. 2007) and accelerated trophoblast apoptosis in preeclampsia (Lee et al. 2005). Immunohistochemical studies of human placenta showed that LOX-1 localized in extravillous trophoblasts of first trimester placentas (Pavan et al. 2004; Fournier et al. 2007) and in syncytiotrophoblasts of normal and preeclamptic term placentas (Lee et al. 2005). However, localization of LOX-1 in animals, especially the mouse—the best-studied mammalian experimental model system—has not been reported. In this study, we describe the clear localization of LOX-1 in murine placenta, as determined by using immunohistochemistry and ISH, and we compared these results with data for human placentas.

Materials and Methods

Sample Collection

C57BL/6 mice were purchased from Japan Crea (Tokyo, Japan). Mice were bred in the Animal Resource Facility at Kumamoto University under specific pathogen-free conditions. All animal procedures were approved by the Animal Research Committee at Kumamoto University, and all procedures conformed to Regulations for Animal Experiments of Kumamoto University. Adult female mice (2–5 months old) were mated with males in the evening and were monitored, starting the next morning, for the appearance of a vaginal plug. Noon on the day in which a vaginal plug was found was said to be 0.5 embryonic day (E0.5). Placentas were isolated at various developmental stages between days E10.5 and E18.5. For better tissue orientation, endometrial and myometrial components were not dissected away from placental disks during dissection. For study of the adult tissue distribution of LOX-1 mRNA, tissues were obtained from 8-week-old male mice.

Human placental tissues at 6–41 weeks of gestation were obtained from healthy pregnant women. Before collecting any such samples, we obtained signed informed consent, with consent documents written according to the Declaration of Helsinki, from all pregnant women in this study. First trimester placentas (6–12 weeks of gestation) and term placentas (37–41 weeks of gestation) were obtained from legal elective abortions and spontaneous vaginal deliveries, respectively.

RT-PCR

RNA isolation and RT were performed as previously described (Kobayashi et al. 2007). A 1-mg sample of total RNA was used to produce cDNA with an Omniscript RT Kit (Qiagen; Valencia, CA). The sequences of PCR primers used were as follows—mouse LOX-1 (522-bp product): forward primer, 5′-GAGCTGCAAACTTTTCAGG-3′, reverse primer, 5′-GTCTTTCATGCAGCAACAG-3′; human LOX-1 (193-bp product): forward primer, 5′-TTACTCTCCATGGTGGTGCC-3′, reverse primer:,5′-AGCTTCTTCTGTTGTTGCC-3′; glyceraldehyde-3-phosphate dehydrogenase (GAPDH; 392-bp product): forward primer, 5′-GGAAAGCTGTGGCGTTGGCGTGAT-3′, reverse primer, 5′-CTGTTGCTGTAGCCGTATTC-3′. These PCR primers were custom-made by Invitrogen (Carlsbad, CA). The primers for GAPDH were designed to be available for both mice and humans.

The PCR cycle parameters were as follows: 15 min at 95C, three-step cycling (denaturation at 94C for 30 sec; annealing at 55–60C for 30 sec; and extension at 72C for 1 min), and 10 min at 72C using an iCycler Thermal Cycler (Bio-Rad Laboratories; Hercules, CA). Thirty cycles were used for LOX-1; 28 cycles were used for GAPDH. Annealing temperatures for LOX-1 and GAPDH were 55C and 60C, respectively. A 10-ml aliquot of each PCR product was subjected to electrophoresis on a 2% (w/v) agarose gel containing 0.1 mg/ml ethidium bromide.

Real-time PCR Analysis

To quantify LOX-1 mRNA levels in murine and human placental tissues, real-time PCR was performed with an ABI PRISM 7700 Sequence Detection System (Applied Biosystems; Foster City, CA) as described earlier (Tsujita et al. 2007). A standard curve was constructed by plotting the relative amounts of a serial dilution of placental cDNA. Mouse placentas were taken from at least three animals at each gestational age of E10.5, E11.5, E13.5, E14.5, E15.5, E16.5, E17.5, and E18.5. For human samples, first trimester placentas (6–12 weeks of gestation, $n=8$) and term placentas (37–41 weeks of gestation, $n=5$) were compared. For measurements, villi were separated from decidua and other components of first trimester placenta using stereoscopic microscopy. Chorionic villi of central cotyledons were collected from term placentas. All experiments were performed in duplicate. Thermal cycler conditions consisted of 2 min at 50C (with uracil *N*-glycosylase for prevention of carryover contamination) and 10 min at 95C (for hot start PCR), followed

by 40 cycles of 15 sec at 95C and 1 min at 60C. Quantitative values of expression of target genes were determined as relative to endogenous 18S rRNA gene expression.

ISH

cRNA probes for mouse and human LOX-1 were synthesized from PCR-generated cDNA as described previously (Divjak et al. 2002) with minor modifications. PCR amplification of template PCR-generated cDNA (2.5 ml) was performed using PrimeSTAR HS DNA Polymerase (Takara; Kyoto, Japan) with the following primer pairs: T7 mouse LOX-1 primer (544-bp product), 5′-CTTAATACGACTCACTATAGGG-GAGCTGCAAACTTTTCAGG-3′ (forward primer) and 5′-CTTAATACGACTCACTATAGGGACAGAT-GTCAAGGCCAACA-3′(reverse primer); T7 human primer (544-bp product), 5′-CT TAATACGACT-CACTATAGGGCTGGAGGGACAGATCTCAGC-3′ (forward primer) and 5′-CTTAATACGACTCACTA-TAGGGTTTCCGCATAAACAGCTCCT-3′ (reverse primer). PCR products were purified by using a High Pure PCR Product Purification Kit (Roche Diagnostics; Mannheim, Germany). Next, purified PCR products were transcribed in vitro by means of T7 RNA polymerase and were labeled with digoxigenin (DIG)-dCTP using a DIG In Vitro Transcription Kit (Roche Diagnostics) to produce sense and antisense cRNA probes. Finally, cRNA probes were purified using a mini Quick Spin RNA column (Roche Diagnostics). Purified cRNA probes were mixed with equal volumes of deionized formamide (Wako; Osaka, Japan).

Murine and human placentas were fixed in 4% paraformaldehyde solution at 4C overnight and were embedded in paraffin. Paraffin sections (3 mm) were deparaffinized in xylene and rehydrated in graded alcohols. Sections were treated with 10 mg/ml proteinase K (Roche Diagnostics) for 10 min at 37C and were post-fixed in 4% paraformaldehyde, treated with 0.1 N HCl, and acetylated with 0.25% acetic anhydride in 0.1 mol/l triethanolamine (pH 8.0) for 10 min. Sections were dehydrated in graded alcohols and air dried. Samples (50 ng) of cRNA probes were mixed with a 50-fold volume of hybridization buffer containing 50% formamide, 10 mM Tris-HCl (pH 7.5), 200 mg/ml tRNA, 1× Denhardt's solution, 600 mM NaCl, 0.25% SDS, 1 mM EDTA (pH 8.0), and 10% dextran sulfate. The hybridization mixture was heat denatured, applied to dried sections, and covered with Parafilm. Hybridization was performed at 50C for 18 hr in a humidified chamber. After hybridization, Parafilm was removed by a brief washing in 5× SSC (1× SSC: 150 mM NaCl plus 15 mM sodium citrate). Sections were washed in 50% formamide plus 2× SSC for 30 min at 50C. After the sections were washed in TNE (10 mM Tris-HCl, pH 7.5, 0.5 M NaCl, and 0.5 mM EDTA) for 10 min at 37C, they were treated with 10 mg/ml RNase A (Roche Diagnostics) for 30 min at 37C. They were again washed in TNE for 10 min at 37C and were stringently washed sequentially: once in 2× SSC and twice in 0.2× SSC for 20 min at 50C. Sections were washed in buffer 1 (100 mM Tris-HCl, pH 7.5, 150 mM NaCl) for 5 min, were incubated with 1.5% blocking reagent (Roche Diagnostics) diluted in buffer 1, and were incubated for 30 min at room temperature with alkaline phosphatase–conjugated rabbit anti-DIG F(ab') fragment antibody (Roche Diagnostics) diluted 1:500 in buffer 1. After sections were washed twice in buffer 1 for 15 min and once in buffer 2 (100 mM Tris-HCl, pH 9.5, 100 mM NaCl, and 50 mM $MgCl_2$) for 5 min, they were covered with 200 ml of buffer 2 containing nitroblue tetrazolium and 5-bromo-4-chloro-2-indolyl phosphate (Roche Diagnostics) and were placed in humidified chambers. Color development was monitored using a light microscope. Dark blue indicated a positive reaction. After a brief washing in tap water, sections were mounted in permanent aqueous medium (Nichirei; Tokyo, Japan). Counterstaining was not performed. Sections incubated with the sense probe served as negative controls.

Histology and Immunohistochemistry

Formalin-fixed paraffin sections were stained with hematoxylin and eosin. Paraffin sections 3 mm thick were used to localize mouse desmin. Endogenous peroxidase activity in murine placental sections was blocked with 0.3% H_2O_2 in 100% methanol for 30 min at room temperature, after which sections were incubated for 90 min at room temperature with anti-human desmin rabbit polyclonal antibody (1 mg/ml, RB-9014-P; Lab Vision, Suffolk, UK), which cross-reacts with mouse desmin. An incubation for 30 min at room temperature with goat anti-rabbit Ig-conjugated peroxidase-labeled polymer amino acid (Nichirei) followed. Peroxidase activity was visualized using 3,3′-diaminobenzidine tetrahydrochloride (Dojin Chemicals; Kumamoto, Japan) as the substrate. Meyer's hematoxylin was used as the counterstain. As a negative control, normal rabbit IgG (10 mg/ml; Santa Cruz Biotechnology, Santa Cruz, CA) was used instead of the primary antibody.

For immunohistochemical studies of LOX-1, murine and human placental tissues were fixed with freshly prepared periodate-lysine-paraformaldehyde (PLP) fixative for 6–8 hr at 4C, after which they were washed with a graded series (10–20%) of sucrose in 0.1 M PBS. Fixed tissues were embedded in tissue-embedding media, frozen in liquid nitrogen, and cut into 6-mm-thick sections. Endogenous peroxidase activity in the murine placental sections was blocked as described above, followed by incubation of the sections for 90 min at room temperature with anti-mouse LOX-1

The Journal of Histochemistry & Cytochemistry

rat monoclonal antibody (JTX-58, rat IgG; 5 mg/ml). Sections were incubated for 30 min at room temperature with goat anti-rat Ig-conjugated peroxidase-labeled polymer amino acid (Nichirei). Visualization of peroxidase activity and counterstaining were performed as described. As a negative control, normal rat IgG (10 mg/ml; Santa Cruz Biotechnology) was used instead of the primary antibody.

To stain human LOX-1, frozen sections of human placental tissues were incubated for 90 min at room temperature with biotinylated anti-human LOX-1 mouse monoclonal antibody (JTX-92, mouse IgG; 6.9 mg/ml). Sections were incubated for 30 min at room temperature with avidin-biotin complex (VECTASTAIN Elite ABC kit; Vector Laboratories, Burlingame, CA). Peroxidase activity was visualized as described above. As a negative control, biotin-conjugated normal mouse IgG (10 mg/ml; Santa Cruz Biotechnology) was used instead of the primary antibody.

Electron Microscopy and Immunoelectron Microscopy

Electron microscopic observation was performed as described previously (Komohara et al. 2005). For immunoelectron microscopy, frozen sections of PLP-fixed murine placentas were incubated overnight at 4C with anti-mouse LOX-1 monoclonal antibody (JTX-58). The sections were washed with PBS, after which they were incubated for 2 hr at 4C with peroxidase-conjugated anti-mouse IgG [(F(ab')2] (Amersham; Buckinghamshire, UK). Peroxidase activity was visualized in the same way as noted above. The samples were processed as previously described (Komohara et al. 2005). Ultrathin sections were evaluated using a Hitachi H-7500 electron microscope (Tokyo, Japan) without counterstaining.

Results

Expression of LOX-1 mRNA in Murine Organs

Using RT-PCR, we examined the expression of LOX-1 mRNA in various organs of the mouse (Figure 1A). The placenta had the highest level of LOX-1 mRNA expression. Lung and aorta showed moderate expression, and expression in other organs was weak or absent. To compare the level of LOX-1 mRNA expression in the placenta at various developmental stages, placental tissues from E10.5 to E18.5 were examined by means of real-time RT-PCR. Expression of LOX-1 mRNA peaked at midgestation (E14.5–E15.5) and decreased thereafter (Figure 1B).

Compartment-specific Expression of LOX-1 mRNA in Murine Placenta

Because strong LOX-1 mRNA expression was observed during midgestational days, placental tissue at E14.5 was used to examine the localization of LOX-1 protein and mRNA. The fundamental morphology of murine placenta is completed by midgestation, with the tissue being compartmentalized into four distinct regions: metrial glands (MG), decidua basalis (DB), junctional zone (JZ), and labyrinth zone (LZ) (Georgiades et al. 2002). The MG and DB belong to the maternal side, whereas the LZ and JZ belong to the fetal side. To examine the compartment-specific expression of LOX-1 mRNA, we separated pregnant uterus and placenta at

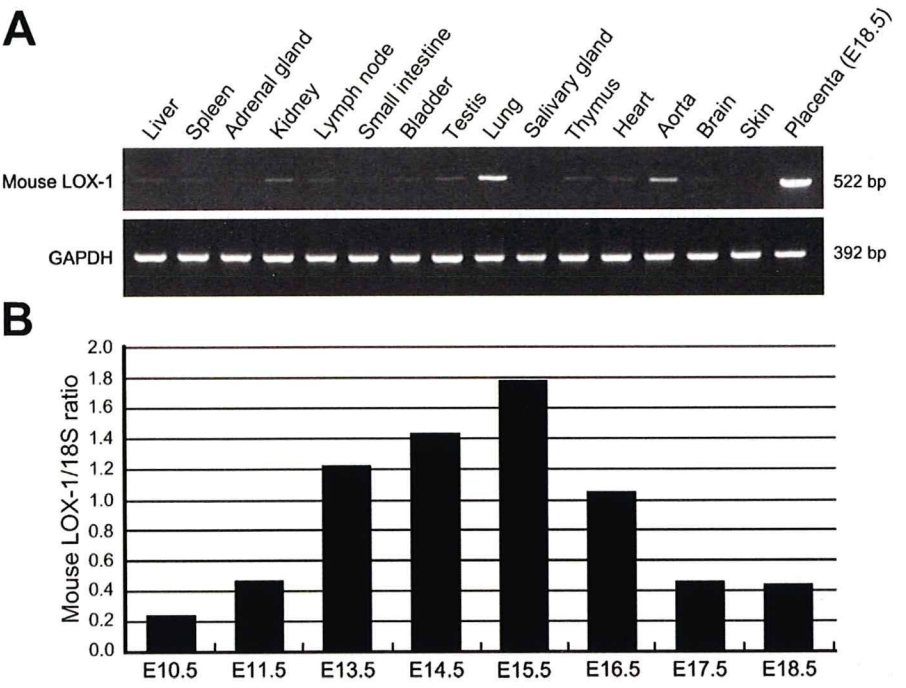

Figure 1 Expression of lectin-like oxidized low-density lipoprotein receptor-1 (LOX-1) mRNA in different murine organs (**A**) and in murine placentas at different gestational days (**B**). Among the organs, the placenta at embryonic day 18.5 (E19.5) had the strongest LOX-1 mRNA expression; lung and aorta showed moderate expression (**A**). By real-time PCR, the placenta at E15.5 had the strongest expression of LOX-1 mRNA, which decreased gradually thereafter (**B**). PCR product sizes were 522 bp for mouse LOX-1 and 392 bp for glyceraldehyde-3-phosphate dehydrogenase (GAPDH).

E14.5 into four parts: myometrium, MG + DB, JZ + LZ, and yolk sac + amnion. RT-PCR analysis showed stronger expression of LOX-1 mRNA in the MG + DB and LZ + JZ compared with the other two parts (Figure 2).

Localization of LOX-1 Protein and mRNA in Different Compartments of Murine Placenta

At E14.5, the four compartments of the murine placenta have distinct histological features (Figure 3A). To clarify the precise localization of LOX-1 expression in each compartment, we used immunohistochemistry and ISH. In agreement with results of RT-PCR analysis, LOX-1 protein was detected in these compartments, with distinct localization patterns. Diffuse LOX-1 staining was observed in the MG and the outer part of the DB (Figure 3B). Strong cord-like staining in the JZ and faint diffuse staining in the LZ were also seen (Figure 3B). No positive staining was observed in a negative control section (Figure 3C). ISH showed clear colocalization of mRNA with the protein in all compartments (Figure 3D). An ISH control section, with the sense probe, showed no positive signal (Figure 3E).

Cellular Localization of LOX-1 Protein and mRNA in Different Compartments of Murine Placenta

In the mouse MG at midgestation, the major cellular components are granulated metrial gland (GMG) cells, also known as uterine natural killer (NK) cells, and fibroblast-like stromal cells. These two cell types are closely associated, with the fibroblast-like cells surrounding large, plump GMG cells (Figure 4A). In immunohistochemical studies, LOX-1 was localized in the fibroblast-like cells but not in GMG cells (Figure 4B). ISH clearly differentiated these two cell types: LOX-1 mRNA was detected in the cytoplasm of the fibroblast-like stromal cells surrounding the GMG cells (Figure 4C). The expression pattern of LOX-1 mRNA in the fibroblast-like cells was in agreement well with that of desmin protein, a marker for this type of cell (Figure 4D). Ultrastructural observation confirmed the intimate association of the fibroblast-like cells and the GMG cells (Figure 4E). Immunoelectron microscopy confirmed dense labeling of the cell membrane of fibroblast-like stromal cells for LOX-1 (Figure 4F).

In the DB, the fibroblast-like cells formed a meshwork around the GMG cells (Figure 5A), but in a rather looser fashion than in the MG. The loose arrangement made it easier to determine that LOX-1–expressing cells were fibroblast-like stromal cells (Figure 5B). Electron and immunoelectron microscopy showed positive LOX-1 staining on plasma membranes of these fibroblast-like cells (Figures 5C and 5D).

After E12.5, clusters of glycogen trophoblast cells with clear cytoplasm were noted among spongiotrophoblasts in the JZ (data not shown). Cord-like clusters of glycogen trophoblasts in the JZ were strongly positive for LOX-1 protein (Figure 5E) and mRNA (Figure 5F). After E14.5, some glycogen trophoblasts crossed the giant cell layer and migrated into the DB, where they were still positive for LOX-1 but at a weaker intensity (Figure 5E). Spongiotrophoblasts and giant trophoblasts showed no positive staining (Figures 5E and 5F). Electron microscopy showed that these glycogen trophoblast cells had a characteristic pale vacuolated cytoplasm (Figure 5G), and LOX-1 was localized along the cell membrane (Figure 5H). In the LZ, weak staining of LOX-1 protein (Figure 5I) and

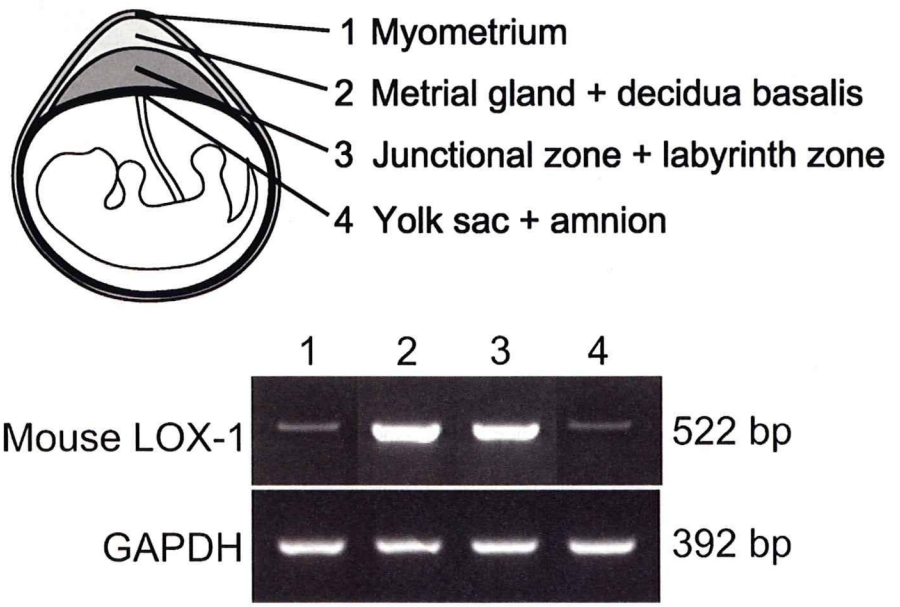

Figure 2 Expression of LOX-1 mRNA in different compartments of murine placenta. For RT-PCR, the placenta (E14.5) was divided into four parts: myometrium, metrial gland (MG) + decidua basalis (DB), junctional zone (JZ) + labyrinth zone (LZ), and yolk sac + amnion. The MG + DB (Lane 2) and the JZ + LZ (Lane 3) showed strong mRNA expression.

The Journal of Histochemistry & Cytochemistry

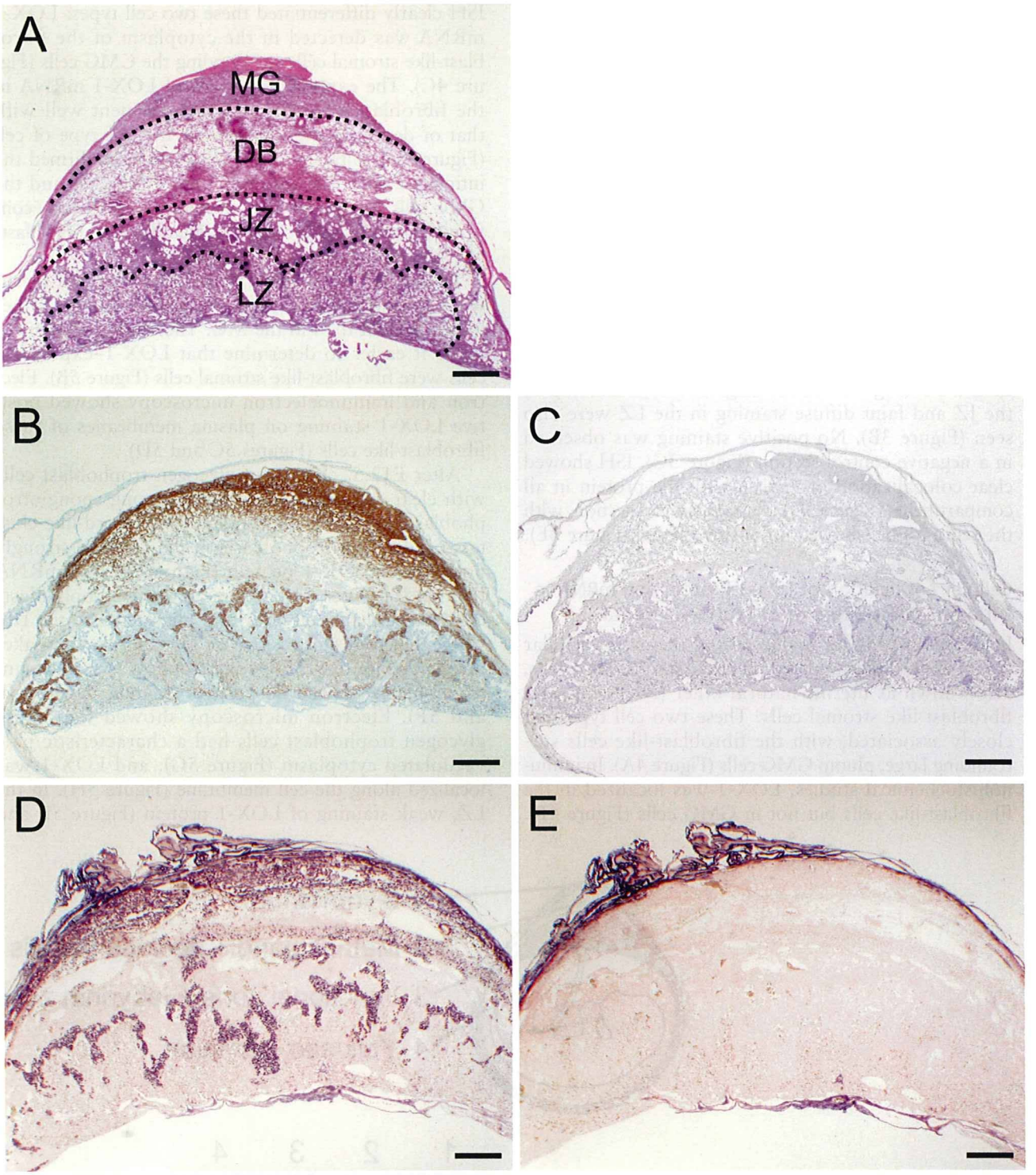

Figure 3 Localization of LOX-1 protein and mRNA in murine placenta at E14.5. Four distinct compartments were easily distinguished by means of hematoxylin and eosin staining (**A**). Immunohistochemistry for LOX-1 (**B**) and ISH for LOX-1 mRNA (**D**) produced very similar localization patterns. The negative control for LOX-1 immunostaining using normal rat IgG showed no staining (**C**). ISH with the sense probe (**E**) showed no positive reaction except for nonspecific staining at the edge of the section. MG, metrial gland; DB, decidua basalis; JZ, junctional zone; LZ, labyrinth zone. Bar = 300 μm.

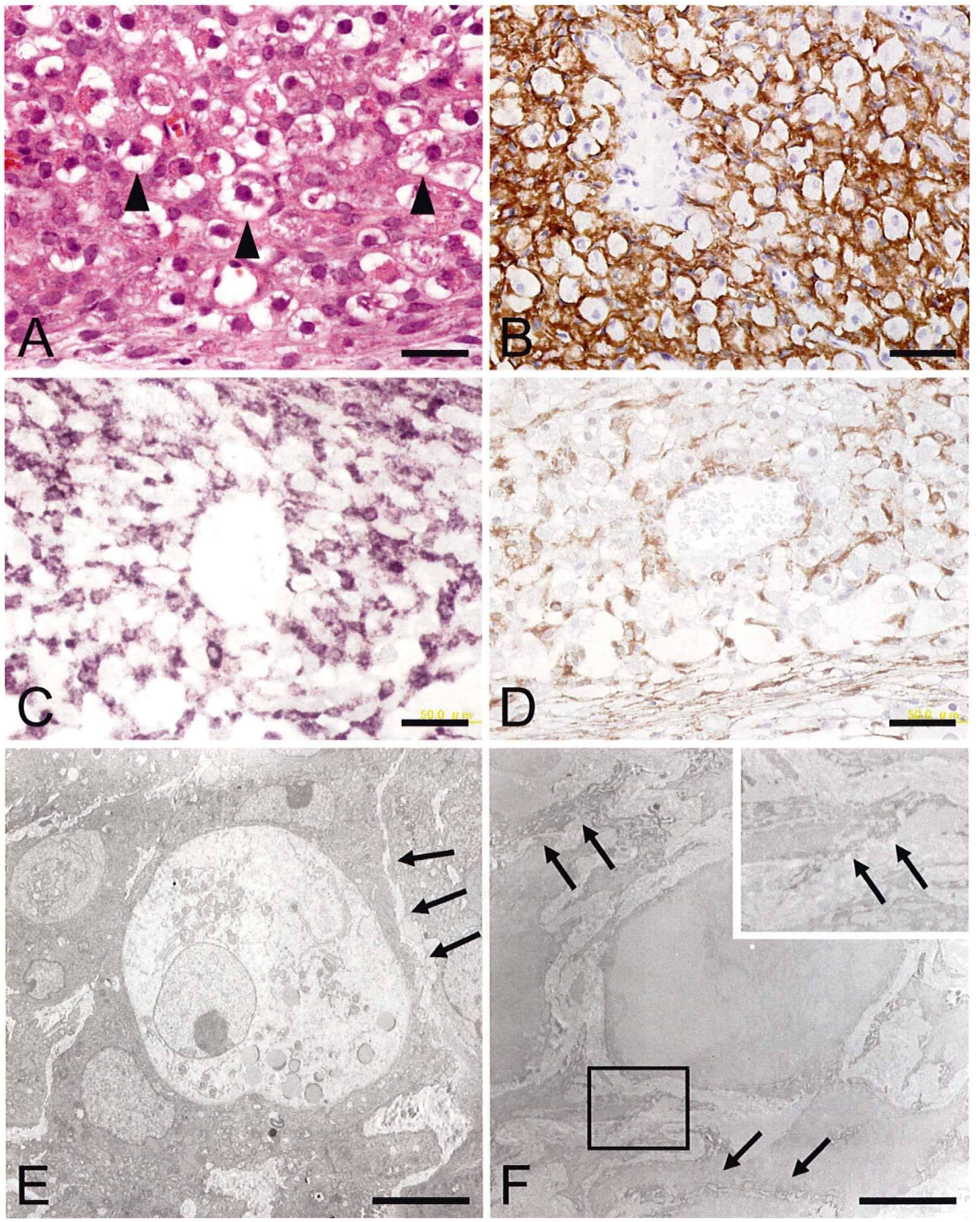

Figure 4 LOX-1–expressing cells in the MG of murine placenta at E14.5. **(A)** In the MG, fibroblast-like cells were closely associated with GMG cells, also known as uterine natural killer (NK) cells (arrowheads; hematoxylin and eosin staining). **(B)** LOX-1 immunostaining was observed on fibroblast-like cells surrounding uterine NK cells. **(C)** LOX-1 mRNA was also detected in fibroblast-like cells by ISH. **(D)** Immunostaining of desmin, a marker for fibroblast-like cells, showed the same localization pattern as did that of LOX-1. **(E)** Electron microscopy showed the close association of a uterine NK cell, which has a characteristic round shape, pale cytoplasm, and fibroblast-like cells surrounding it, with long cell processes of the fibroblast-like cells (arrows). **(F)** An immunoelectron micrograph showed distinct localization of reaction products of LOX-1 on cell processes of fibroblast-like cells (arrows). Inset in **F** is the higher-magnification image of the boxed area. Bars: **A–D** = 50 μm; **E,F** = 10 μm.

The Journal of Histochemistry & Cytochemistry

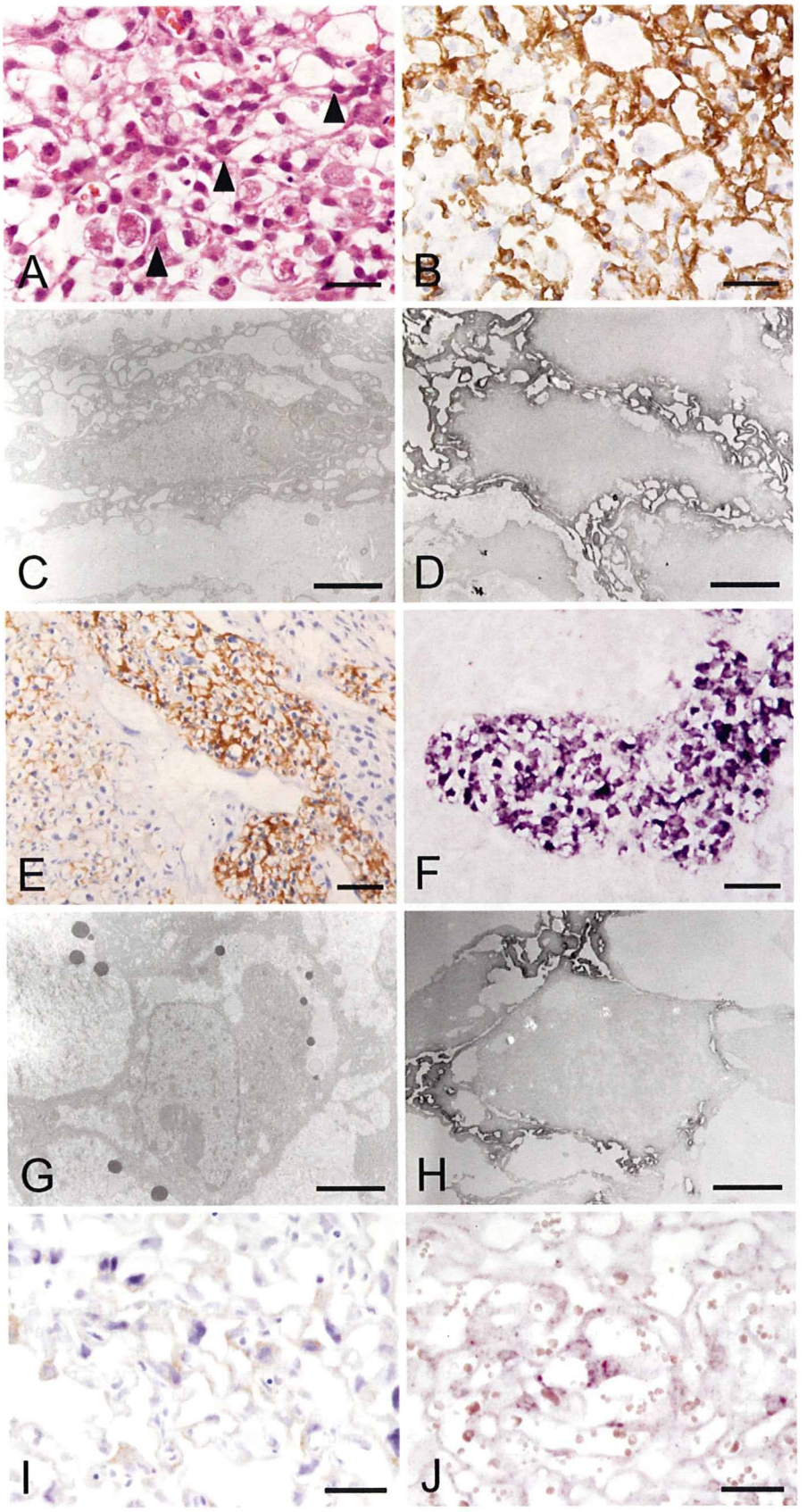

Figure 5 LOX-1–expressing cells in the DB, JZ, and LZ of murine placenta at E14.5. **(A)** In the DB, fibroblast-like stromal cells (arrowheads) formed a meshwork and surrounded uterine NK cells in a looser fashion than in the MG. **(B)** Immunohistochemical LOX-1 localization coincided with the mesh-like structure of the fibroblast-like cells. Electron **(C)** and immunoelectron **(D)** microscopy showed distinct localization of LOX-1 on well-developed cell processes of the fibroblast-like cells. In the JZ, clusters of glycogen trophoblast cells had a strongly positive reaction for LOX-1 protein along their cell membranes **(E)** and for LOX-1 mRNA **(F)**, whereas cells in the DB had a weaker reaction **(E)**. Electron **(G)** and immunoelectron **(H)** microscopy showed strong LOX-1 immunoreactivity along the well-developed cell processes of glycogen trophoblast cells. In the LZ, weak staining of LOX-1 protein **(I)** and weak mRNA expression **(J)** were found in labyrinthine cytotrophoblasts. Bars: **A,B,E,F,I, J** = 50 μm; **C,D** = 2.5 μm; **G,H** = 5.0 μm.

The Journal of Histochemistry & Cytochemistry

weak mRNA expression (Figure 5J) were shown in labyrinthine cytotrophoblasts.

From these data, we concluded that, in the maternal compartment, LOX-1 localized in fibroblast-like stromal cells, whereas in the fetal compartment, LOX-1 was strongly expressed in glycogen trophoblast cells and weakly expressed in labyrinthine cytotrophoblasts.

Expression of LOX-1 mRNA in Human Placenta

To compare the expression levels of LOX-1 mRNA in first trimester and term human placentas, we performed real-time RT-PCR. Significantly stronger expression of LOX-1 mRNA was found in first trimester placenta compared with term placenta (Figure 6).

Identification of LOX-1–expressing Cells in Human Placenta

In the first trimester human placenta, strong positive immunoreactivity for LOX-1 was seen along the cell membrane of most villous cytotrophoblasts but not in syncytiotrophoblasts (Figure 7A). No positive staining was observed in a negative control section (Figure 7B). ISH of a first trimester placenta showed a positive reaction for LOX-1 mRNA in villous cytotrophoblasts (Figures 7B and 7C). The localization pattern of LOX-1 did not change in the term placenta. Lox-1 is positive on flattened cytotrophoblasts located beneath the syncytiotrophoblasts (Figure 7E). No staining was observed in a control section (Fig. 7F).

Discussion

Since the discovery of LOX-1 by Sawamura et al. (1997), many reports have suggested its possible involvement in the pathogenesis of atherosclerosis (Mehta et al. 2006). Recently, Mehta et al. (2007) reported that deletion of LOX-1 in atherogenic LDL receptor knockout mice reduced atherosclerosis and proinflammatory and prooxidant signals. LOX-1 expression is enhanced in some proatherogenic settings such as hypertension and hyperlipidemia in vivo and in atherosclerotic lesions (Mehta et al. 2006). LOX-1 is expressed at very low levels in healthy endothelium (Sawamura et al. 1997), and the physiological role of LOX-1 is not well understood. Northern blotting data for normal mice and humans (Sawamura et al. 1997) showed that the placenta is the organ with the greatest expression of LOX-1 mRNA, which indicates that LOX-1 may play an important role in maintaining pregnancy.

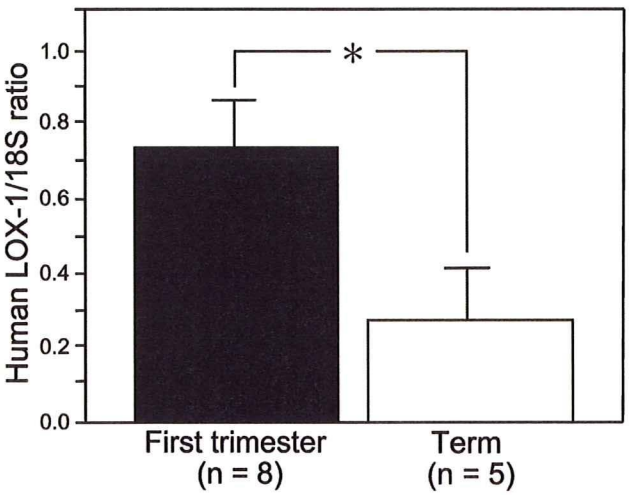

Figure 6 Expression of LOX-1 mRNA in human placenta. Real-time PCR showed significantly greater LOX-1 mRNA expression in the first trimester placenta than in the term placenta (*$p<0.05$).

During pregnancy, the placenta is a major source of prooxidant and endogenous antioxidant synthesis (Walsh 1998). Excessive generation of free radicals depletes antioxidant pools and causes oxidative damage to lipids, proteins, and DNA. The level of placental oxidative stress increases rapidly at the end of the first trimester, when placental vascular development is occurring, and such stress tapers off later in gestation (Jauniaux et al. 2000). Our present finding of higher expression of LOX-1 mRNA during early and mid-gestational stages compared with late gestation in both mouse and human indicates induction of LOX-1 by increased oxidative stress at this gestational stage and active involvement of LOX-1 in the functioning of early gestational stage placenta.

In maternal decidual compartments of murine placenta, namely the MG and DB, the major cellular components are vascular endothelial cells, uterine NK cells (GMG cells), and fibroblast-like stromal cells. It is interesting to note that LOX-1 localized in fibroblast-like cells—the cells that are closely associated with uterine NK cells—but not in vascular endothelial cells. Certain studies indicate the possible role of uterine NK cells in control of trophoblast invasion and remodeling of uterine spiral arteries during the first half of pregnancy (Bulmer and Lash 2005). Intimate association between uterine NK cells and fibroblast-like stromal cells is believed to be important for survival of the uterine NK cells (Stewart 2000). Because ox-LDL binding of LOX-1 in fibroblasts induces expression of various adhesion molecules, such as intercellular adhesion molecule-1 and vascular cell adhesion molecule-1 (Chen et al. 2005), LOX-1 may be involved in strengthening the close association of these cells. The number of uterine NK cells decreases in late pregnancy, and apoptotic uterine NK cells were observed at day 16 in rat placenta, with their number increasing thereafter (Fukazawa et al. 1998). Because LOX-1 functions in the elimination of aged or apoptotic cells (Oka et al. 1998), LOX-1 expression by fibroblast-like stromal cells may also contribute to the elimination of apoptotic uterine NK cells.

The Journal of Histochemistry & Cytochemistry

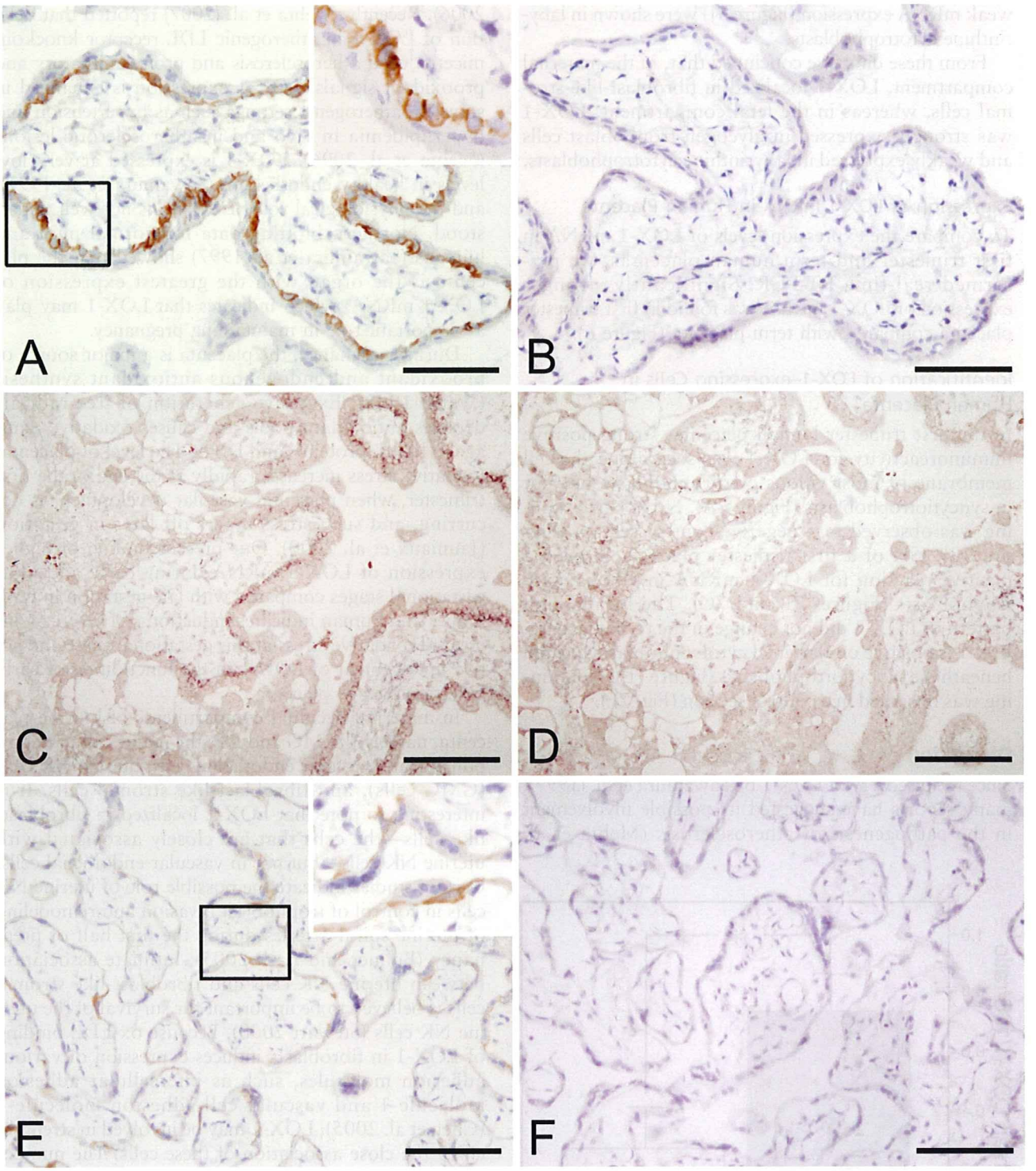

Figure 7 **(A)** LOX-1 immunostaining is observed along the cell membrane of cuboidal villous cytotrophoblasts of a first trimester placenta (9 weeks). Inset is the higher-magnification image of the boxed area. **(B)** No positive staining is observed in a negative control section using normal mouse IgG. **(C)** LOX-1 mRNA is detected in the cytoplasm of cytotrophoblasts in the first trimester placenta (9 weeks). **(D)** The control section with the sense probe showed no positive reaction. **(E)** In the term placenta, the flattened cytotrophoblast layer is positive for LOX-1 immunostaining. Inset, the higher-magnification image of the boxed area, shows LOX-1–positive cytotrophoblasts subjacent to LOX-1–negative syncytiotrophoblasts. **(F)** No positive reaction is observed in a control section using normal mouse IgG. Bars: **A–D** = 100 μm; **E,F** = 50 μm.

In the JZ and LZ, LOX-1 expression was restricted to glycogen trophoblast cells. Glycogen trophoblast cells are of undetermined origin that arise in the JZ (Fukazawa et al. 1998). Although these cells were once thought to be differentiated from spongiotrophoblasts (Adamson et al. 2002; Georgiades et al. 2002), more recent evidence suggests that they are distinct from spongiotrophoblasts (Rampon et al. 2005; Bouillot et al. 2006). Because we found no LOX-1 expression in spongiotrophoblasts at the mRNA and protein levels, we believe that LOX-1 is one of the molecules that discriminates between glycogen trophoblast cells and spongiotrophoblasts.

This is the first study to describe the distinct localization of LOX-1 in murine placenta. It is interesting to note that LOX-1 expression is not observed in vascular endothelial cells of murine placenta. Because vascular endothelial cells are a major cell type for LOX-1 expression in the lung, aorta, and other organs (Sawamura et al. 1997), LOX-1 expressed by fibroblast-like stromal cells and glycogen trophoblast cells may possess unique functions in murine placenta.

Because glycogen trophoblast cells invade decidua, they are considered to be analogous to the human invasive extravillous trophoblasts (Malassine et al. 2003; Coan et al. 2006). Pavan et al. (2004) reported that ox-LDL, but not native LDL, inhibited human extravillous trophoblast invasion in a concentration-dependent manner, as evidenced in the trophoblast invasion assay. They also discovered that LOX-1 was the main scavenger receptor responsible for uptake of ox-LDL by cytotrophoblasts (Pavan et al. 2004). Taking these data together, LOX-1 expression by glycogen trophoblast cells may regulate their invasion of the DB. The weaker expression of LOX-1 by invading glycogen trophoblast cells in the DB, which we observed, supports this hypothesis.

In the first trimester placenta of humans, we confirmed the localization of LOX-1 in villous cytotrophoblasts but not syncytiotrophoblasts nor vascular endothelial cells by means of immunohistochemistry and ISH. We also found LOX-1 localization in villous cytotrophoblasts in term placentas. Our result in term placenta is inconsistent with the previous observation by Lee et al. (2005), who observed LOX-1 expression in syncytiotrophoblasts in normal term and preeclamptic placentas, with stronger staining in the latter. LOX-1 staining in Figure 3 of their report (Lee et al. 2005), however, seems to localize in the cytotrophoblast layer. In a recent study, Mori et al. (2007) reported that the cytotrophoblast layer in the term placenta becomes thinner by spreading their cell surface over the basal lamina, and 80% of its continuity is still preserved. Our data of LOX-1 localization in term placenta support their observation.

For the murine placenta, we clearly showed that LOX-1–expressing cells were fibroblast-like stromal cells in the MG and DB and glycogen trophoblast cells in the JZ and LZ, as well as labyrinthine cytotrophoblasts in the LZ. LOX-1 does not seem to be essential to maintain placental function, because LOX-1–deficient mice were fertile (Mehta et al. 2007) and had no detectable abnormal pregnancy. However, LOX-1–expressing placental cells may be involved in management of oxidative stress during pregnancy. Further study is needed, however, to clarify the exact role of LOX-1 in pregnancy.

Acknowledgments

This study was supported in part by Grants-in-Aid for Scientific Research (B16390108, C17590797) from the Ministry of Education, Culture, Sports, Science, and Technology of Japan.

Literature Cited

Adamson SL, Lu Y, Whiteley KJ, Holmyard D, Hemberger M, Pfarrer C, Cross JC (2002) Interactions between trophoblast cells and the maternal and fetal circulation in the mouse placenta. Dev Biol 250:358–373

Aoyama T, Chen M, Fujiwara H, Masaki T, Sawamura T (2000) LOX-1 mediates lysophosphatidylcholine-induced oxidized LDL uptake in smooth muscle cells. FEBS Lett 467:217–220

Aoyama T, Fujiwara H, Masaki T, Sawamura T (1999) Induction of lectin-like oxidized LDL receptor by oxidized LDL and lysophosphatidylcholine in cultured endothelial cells. J Mol Cell Cardiol 31:2101–2114

Bonet B, Chait A, Gown AM, Knopp RH (1995) Metabolism of modified LDL by cultured human placental cells. Atherosclerosis 112:125–136

Bouillot S, Rampon C, Tillet E, Huber P (2006) Tracing the glycogen cells with protocadherin 12 during mouse placenta development. Placenta 27:882–888

Branch DW, Mitchell MD, Miller E, Palinski W, Witztum JL (1994) Pre-eclampsia and serum antibodies to oxidized low-density lipoprotein. Lancet 343:645–646

Bulmer JN, Lash GE (2005) Human uterine natural killer cells: a reappraisal. Mol Immunol 42:511–521

Burton GJ, Jauniaux E (2004) Placental oxidative stress: from miscarriage to preeclampsia. J Soc Gynecol Investig 11:342–352

Chen K, Chen J, Liu Y, Xie J, Li D, Sawamura T, Hermonat PL, et al. (2005) Adhesion molecule expression in fibroblasts: alteration in fibroblast biology after transfection with LOX-1 plasmids. Hypertension 46:622–627

Chen M, Nagase M, Fujita T, Narumiya S, Masaki T, Sawamura T (2001) Diabetes enhances lectin-like oxidized LDL receptor-1 (LOX-1) expression in the vascular endothelium: possible role of LOX-1 ligand and AGE. Biochem Biophy Res Commun 287:962–968

Coan PM, Conroy N, Burton GJ, Ferguson-Smith AC (2006) Origin and characteristics of glycogen cells in the developing murine placenta. Dev Dyn 235:3280–3294

Divjak M, Glare EM, Walters EH (2002) Improvement of non-radioactive in situ hybridization in human airway tissues: use of PCR-generated templates for synthesis of probes and an antibody sandwich technique for detection of hybridization. J Histochem Cytochem 50:541–548

Draude G, Hrboticky N, Lorenz RL (1999) The expression of the lectin-like oxidized low-density lipoprotein receptor (LOX-1) on human vascular smooth muscle cells and monocytes and its down-regulation by lovastatin. Biochem Pharmacol 57:383–386

Fournier T, Handschuh K, Tsatsaris V, Evain-Brion D (2007) Involvement of PPARg in human trophoblast invasion. Placenta 28(suppl A):S76–81

The Journal of Histochemistry & Cytochemistry

Fukazawa Y, Yamamura Y, Sato T, Iguchi T, Ohta Y (1998) Mode of cell death in the rat metrial gland during peripartum regression. Anat Rec 252:369–377

Georgiades P, Ferguson-Smith AC, Burton GJ (2002) Comparative developmental anatomy of the murine and human definitive placentae. Placenta 23:3–19

Hubel CA (1999) Oxidative stress in the pathogenesis of preeclampsia. Proc Soc Exp Biol Med 222:222–235

Jauniaux E, Watson AL, Hempstock J, Bao YP, Skepper JN, Burton GJ (2000) Onset of maternal arterial blood flow and placental oxidative stress. A possible factor in human early pregnancy failure. Am J Pathol 157:2111–2122

Kobayashi H, Sakashita N, Okuma T, Terasaki Y, Tsujita K, Suzuki H, Kodama T, et al. (2007) Class A scavenger receptor (CD204) attenuates hyperoxia-induced lung injury by reducing oxidative stress. J Pathol 212:38–46

Komohara Y, Terasaki Y, Kaikita K, Suzuki H, Kodama T, Takeya M (2005) Clearance of apoptotic cells is not impaired in mouse embryos deficient in class A scavenger receptor types I and II (CD204). Dev Dyn 232:67–74

Kume N, Murase T, Moriwaki H, Aoyama T, Sawamura T, Masaki T, Kita T (1998) Inducible expression of lectin-like oxidized LDL receptor-1 in vascular endothelial cells. Circ Res 83:322–327

Lee H, Park H, Kim YJ, Kim HJ, Ahn Y-M, Park B, Park JH, et al. (2005) Expression of lectin-like oxidized low-density lipoprotein receptor-1 (LOX-1) in human preeclamptic placenta: possible implications in the process of trophoblast apoptosis. Placenta 26:226–233

Li D, Mehta JL (2000) Upregulation of endothelial receptor for oxidized LDL (LOX-1) by oxidized LDL and implications in apoptosis of human coronary artery endothelial cells. Arterioscler Thromb Vasc Biol 20:1116–1122

Li DY, Zhang YC, Philips MI, Sawamura T, Mehta JL (1999) Upregulation of endothelial receptor for oxidized low-density lipoprotein (LOX-1) in cultured human coronary artery endothelial cells by angiotensin II type 1 receptor activation. Circ Res 84: 1043–1049

Malassine A, Frendo J-L, Evain-Brion D (2003) A comparison of placental development and endocrine functions between the human and mouse model. Hum Reprod Update 9:531–539

Mehta JL, Chen J, Hermonat PL, Romeo F, Novelli G (2006) Lectin-like, oxidized low-density lipoprotein receptor-1 (LOX-1): a critical player in the development of atherosclerosis and related disorders. Cardiovasc Res 69:36–45

Mehta JL, Sanada N, Hu CP, Chen J, Dandapat A, Sugawara F, Satoh H, et al. (2007) Deletion of LOX-1 reduces atherogenesis in LDLR knockout mice fed high cholesterol diet. Circ Res 100: 1634–1642

Mori M, Ishikawa G, Luo S-S, Mishima T, Goto T, Robinson JM, Mtsubara S, et al. (2007) The cytotrophoblast layer of human ghorionic villi becomes thinner but maintains its structural integrity during gestation. Biol Reprod 76:164–172

Moriwaki H, Kume N, Kataoka H, Murase T, Nishi E, Sawamura T, Masaki T, et al. (1998a) Expression of lectin-like oxidized low density lipoprotein receptor-1 in human and murine macrophages: upregulated expression by TNF-α. FEBS Lett 440:29–32

Moriwaki H, Kume N, Sawamura T, Aoyama T, Hoshikawa H, Ochi H, Nishi E, et al. (1998b) Ligand specificity of LOX-1, a novel endothelial receptor for oxidized low density lipoprotein. Arterioscler Thromb Vasc Biol 18:1541–1547

Nakagawa T, Akagi M, Hoshikawa H, Chen M, Yasuda T, Mukai S, Ohsawa K, et al. (2002) Lectin-like oxidized low-density lipoprotein receptor 1 mediates leukocyte infiltration and articular cartilage destruction in rat zymosan-induced arthritis. Arthritis Rheum 46:2486–2494

Oka K, Sawamura T, Kikuta K, Itokawa S, Kume N, Kita T, Masaki T (1998) Lectin-like oxidized low-density lipoprotein receptor 1 mediates phagocytosis of aged/apoptotic cells in endothelial cells. Proc Natl Acad Sci USA 95:9535–9540

Pavan L, Hermouet A, Tsatsaris V, Therond P, Sawamura T, Evain-Brion D, Fournier T (2004) Lipids from oxidized low-density lipoprotein modulate human trophoblast invasion: involvement of nuclear liver X receptors. Endocrinology 145:4583–4591

Rampon C, Prandini MH, Bouillot S, Pointu H, Tillet E, Frank R, Vernet M, et al. (2005) Protocadherin 12 (VE-cadherin 2) is expressed in endothelial, trophoblast, and mesangial cells. Exp Cell Res 302:48–60

Sawamura T, Kume N, Aoyama T, Moriwaki H, Hoshikawa H, Aiba Y, Tanaka T, et al. (1997) An endothelial receptor for oxidized low-density lipoprotein. Nature 386:73–77

Stewart IJ (2000) Mouse granulated metrial gland cells require contact with stromal cells to maintain viability. J Anat 197:495–502

Tsujita K, Kaikita K, Hayasaki T, Honda T, Kobayashi H, Sakashita N, Suzuki H, et al. (2007) Targeted deletion of class A macrophage scavenger receptor increases the risk of cardiac rupture after experimental myocardial infarction. Circulation 115:1904–1911

Tulppala M, Ailus K (1995) Antibodies to oxidized low-density lipoprotein and to cardiolipin in nonpregnant and pregnant women with habitual abortion. Fertil Steril 64:947–950

Walsh SW (1998) Maternal-placental interactions of oxidative stress and antioxidants in preeclampsia. Semin Reprod Endocrinol 16:93–104

Yoshida H, Kondratenko N, Green S, Steinberg D, Quehenberger O (1998) Identification of the lectin-like receptor for oxidized low-density lipoprotein in human macrophages and its potential role as a scavenger receptor. Biochem J 334:9–13

The Journal of Histochemistry & Cytochemistry

Archives of Biochemistry and Biophysics 479 (2008) 1–14

Contents lists available at ScienceDirect

Archives of Biochemistry and Biophysics

journal homepage: www.elsevier.com/locate/yabbi

LDL protein nitration: Implication for LDL protein unfolding

Ryan T. Hamilton [a], Liana Asatryan [a], Jon T. Nilsen [a], Jose M. Isas [c], Timothy K. Gallaher [a], Tatsuya Sawamura [d], Tzung K. Hsiai [b,*]

[a] Department of Pharmacology and Pharmaceutical Sciences, School of Pharmacy, University of Southern California, Los Angeles, CA 90089, USA
[b] Department of Biomedical Engineering and Division of Cardiovascular Medicine, Viterbi School of Engineering, University of Southern California, Los Angeles, CA 90089, USA
[c] Department of Biochemistry and Molecular Biology, Keck School of Medicine, University of Southern California, Los Angeles, CA 90089, USA
[d] Department of Pharmaceutical Sciences and Division of Cell Biology, Department of Bioscience, National Cardiovascular Center Research Institute, Osaka University, Japan

ARTICLE INFO

Article history:
Received 12 December 2007
and in revised form 12 July 2008
Available online 7 August 2008

Keywords:
LDL
Nitration
Oxidation
Endothelial cells

ABSTRACT

Oxidatively- or enzymatically-modified low-density lipoprotein (LDL) is intimately involved in the initiation and progression of atherosclerosis. The *in vivo* modified LDL is electro-negative (LDL^-) and consists of peroxidized lipid and unfolded apoB-100 protein. This study was aimed at establishing specific protein modifications and conformational changes in LDL^- assessed by liquid chromatography/tandem mass spectrometry (LC/MS/MS) and circular dichroism analyses, respectively. The functional significance of these chemical modifications and structural changes were validated with binding and uptake experiments to- and by bovine aortic endothelial cells (BAEC).

The plasma LDL^- fraction showed increased nitrotyrosine and lipid peroxide content as well as a greater cysteine oxidation as compared with native- and total-LDL. LC/MS/MS analyses of LDL^- revealed specific modifications in the apoB-100 moiety, largely involving nitration of tyrosines in the α-helical structures and β_2 sheet as well as cysteine oxidation to cysteic acid in β_1 sheet. Circular dichroism analyses showed that the α-helical content of LDL^- was substantially lower (~25%) than that of native LDL (~90%); conversely, LDL^- showed greater content of β-sheet and random coil structure, in agreement with unfolding of the protein. These results were mimicked by treatment of LDL subfractions with peroxynitrite ($ONOO^-$) or SIN-1: similar amino acid modifications as well as conformational changes (loss of α-helical structure and gain in β-sheet structure) were observed. Both LDL^- and $ONOO^-$-treated LDL showed a statistically significant increase in binding and uptake to- and by BAEC compared to native LDL. We further found that most binding and uptake in control-LDL was through LDL-R with minimal oxLDL-R-dependent uptake. $ONOO^-$-treated LDL was significantly bound and endocytosed by LOX-1, CD36, and SR-A with minimal contribution from LDL-R.

It is suggested that lipid peroxidation and protein nitration may account for the mechanisms leading to apoB-100 protein unfolding and consequential increase in modified LDL binding and uptake to and by endothelial cells that is dependent on oxLDL scavenger receptors.

Low density lipoprotein (LDL)[1] particles transport cholesterol, cholesterol esters, lipids, phospholipids, and are involved in the maintenance of membrane fluidity [1]. The LDL particle is comprised of lipid core and an apolipoprotein B-100 (apoB-100) moiety. The latter assumes a pentapartite structure with alternating α-helices and β-pleated sheets (α_1–β_1–α_2–β_2–α_3) [2]. α_1 anchors the protein to the lipid core; α_2 and α_3 expand and contract across the phospholipid belt of the LDL particle to stabilize electrostatic interactions, thus maintaining LDL protein structural integrity. β-sheets are structurally rigid and engaged in electrostatic interactions with the phospholipids [2].

It is widely recognized that oxidative and/or enzyme-mediated modifications of LDL are required for the particle to acquire the inflammatory properties inherent in the initiation and progression of atherosclerosis [3,4]. This notion is strengthened by the observation that post-translational modifications of apo-B100 are elevated in atherosclerotic lesions [5]. Oxidation of LDL can be carried out by transition metals, hemoglobin, myeloperoxidase, cerruloplasmin, and reactive oxygen species generated by vascular endothelium [6–8]. The oxidative modifications render the LDL particle electronegatively charged (LDL^-) as compared to native LDL (nLDL) [3,9,10]. Also, LDL^- (*in vivo* oxidatively-modified LDL) contains elevated level of lipid peroxides and aldehydes that are implicated in

* Corresponding author. Fax: +1 323 821 3897.
E-mail address: hsiai@usc.edu (T.K. Hsiai).

[1] *Abbreviations used:* LDL, low-density lipoprotein; nLDL, native LDL; tLDL, total LDL; LDL^-, negatively-charged LDL, oxidatively-modified LDL; CD, circular dichroism; SIN-1, 3-morpholino-sydnonimine; DiI, 3,3,3′,3′-tetramethylindocarbocyanine perchlorate; BAEC, bovine aortic endothelial cells; Apolipoprotein B-100, ApoB-100; LC/EIS/MS, liquid chromatography electron ion spray mass spectrometry.

0003-9861/$ - see front matter © 2008 Elsevier Inc. All rights reserved.
doi:10.1016/j.abb.2008.07.026

protein unfolding [11]. Reactive nitrogen species, especially peroxynitrite ($ONOO^-$), generated by the vascular endothelium, nitrate apo-B-100 in LDL particles [10,12–15]. Enzyme-mediated modifications of LDL—accomplished through the action of ubiquitous hydrolytic enzymes—confer atherogenic properties to the lipoprotein particles [4,16]: *s*-phospholipase A_2 [3] and its free fatty acid product [17], cholesteryl esterases [4], plasmin [18], and matrix metalloproteinase -2 and -9 [18].

This oxidative- and/or enzymatically-modified LDL possesses inflammatory properties: it activates cytokines [19] and monocyte adhesion molecules [20]. The LDL particle is internalized by cells via the ubiquitously expressed LDL receptor (LDL-R). Rather than binding to the LDL-R commonly present in cells, protein unfolding in modified LDL promotes binding to the scavenger receptors (LDL-SR) in vascular endothelial cells [21] and to CD36 in macrophages [11,22]. $ONOO^-$-modified LDL is recognized by macrophages, thus gaining further relevance in endothelial dysfunction and initiation of atherosclerosis [15,23,24]. Further, endothelial cells are involved in the initiation of atherosclerosis by the binding of modified LDL and/or apoptotic cells and inducing macrophage/monocyte chemoattractant proteins as well as inducing inflammation [25].

In this study, we assessed specific protein modifications and conformational changes of *in vivo* oxidatively-modified LDL (LDL^-) and $ONOO^-$-treated LDL by liquid chromatography/tandem mass spectrometry (LC/MS/MS) analyses and circular dichroism (CD) spectra. The significance of $ONOO^-$-driven modifications is underscored by the implication of both NADPH oxidase (a source of $O_2^{\cdot -}$) [10,26,27] and eNOS (a source of ·NO) [28] activities in vascular endothelial dysfunction and by the fast reaction of $O_2^{\cdot -}$ and ·NO to yield $ONOO^-$.

Materials and methods

Chemicals

$ONOO^-$ and monoclonal nitrotyrosine antibody were purchased from Upstate Cell Signaling Solutions (UCSS, Lake Placid, NY). Bovine serum albumin, 3-morpholino-sydnonimine (SIN-1), biotin, and 3′-tetramethylindocarbocyanine perchlorate (DiI) were purchased from Sigma (St. Louis, MO). Bovine aortic endothelial cells were purchased from Cell Applications, Inc. (San Diego, CA). Lectin, like oxidized LDL receptor, was a gift from Dr. Tatsuya Sawamura (Osaka University, Japan). CD36 receptor blocking antibody, SR-A receptor blocking antibody, and LDL-R antibody were obtained from Beckman Coultier (Fullerton, California), Serotec (Raleigh, North Carolina), and Calbiochem (San Diego, California), respectively.

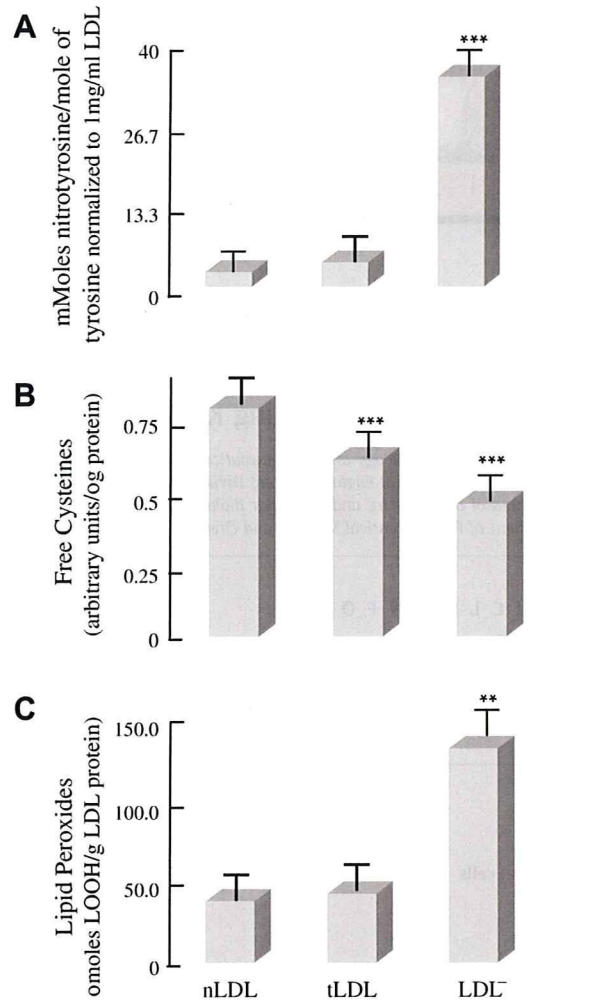

Fig. 1. Chemical modifications of *in vivo* LDL subfractions. LDL sub-fractions were isolated by anion exchange chromatography as described in Materials and methods and analyzed for (A) nitrotyrosine content, (B) free cysteine content (biotin labeling), and labeling, and (C) lipid peroxide content. ($n = 3$, $^*P < 0.05$, $^{**}P < 0.01$, $^{***}P < 0.001$).

Table 1
LC/MS/MS analyses of LDL^- Apo-B100 protein modifications

Secondary structure	Peptide	Modified AA	Sequence	MSc	Charge	XC	Δcn	Modification	% modified
α_1	276–287	NO_2–Tyr^{276}	y[a]gmvaqvtqtlk	51	2	2.8	0.4	nitrotyrosine	100 ± 0
α_1	580–589	NO_2–Trp^{583}	lVQilpw[a]eqneqv	30	2	3.0	0.2	nitrotryptophan	49.8 ± 0.6
α1	580–589	HO–Trp^{583}	lVQilpw[a]eqneqv	38	2	3.8	0.3	hydroxytryptophan	32.6 ± 1.9
α_1	655–669	NO_2–Tyr^{666}	iegnlifdpnny[a]lpk	46	2	3.3	0.4	nitrotyrosine	18.3 ± 0.7
α_1	718–732	NO_2–Tyr^{720}	aly[a]wavngqvpdgvsk	49	2	2.4	0.1	nitrotyrosine	29.9 ± 0.07
β_1	1101–115	SO_3H–Cys^{1112}	itevalmghlsc[a]dtk	84	2	4.9	0.5	cysteic acid	100 ± 0
α_2	2523–2534	NO_2–Tyr^{2524}	my[a]qmdiqqelqr	36	2	3.0	0.3	nitrotyrosine	87.1 ± 0.2
β_2	3137–3148	NO_2–Tyr^{3139}	lpy[a]tiitpplk	30	2	1.9	0.5	nitrotyrosine	60.2 ± 0.2
β_2	3292–3311	NO_2–Tyr^{3295}	vpsy[a]tlilpslelpvlhvpr	70	2	5.6	0.5	nitrotyrosine	80.4 ± 0.2
β_2	3481–3497	NO_2–Tyr^{3489}	lslesltsy[a]fsiesstk	62	2	4.7	0.7	nitrotyrosine	27.1 ± 1.1
β_2	3953–3973	HO–Phe^{3965}	dfsaeyeedgkf[a]eglqewegk	59	2	2.5	0.5	HO-phenylalanine	92.6 ± 0.9
α_3	4133–4145	NO_2–Tyr^{4141}	aasgttgty[a]qewk	46	2	2.7	0.1	nitrotyrosine	81.8 ± 0.1
			Quantification of NO_2-Y mmol NO_2-Y/(mol Y) LDL^- = 34.8 ± 1.0 tLDL = 2.0 ± 0.2 nLDL = 0.3 ± 0.1						

[a] Full annotated MS spectra are represented in the order presented in this table in Figs. 1–12 of the Supplemental section.

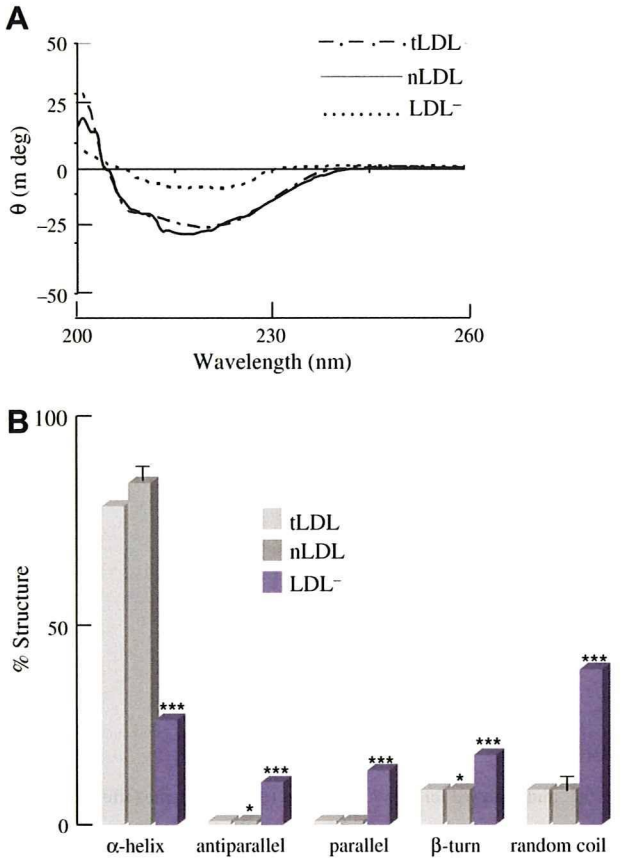

Fig. 2. Circular dichroism spectral analyses of *in vivo* LDL sub-fractions. (A) Circular dichroism spectra for different LDL sub-fractions were performed as described in Materials and methods. (B) Secondary structures of LDL sub-fractions; data were obtained from spectra in (A), which were deconvoluted for apoB-100 secondary structure. ($n = 3$, $^{*}P < 0.05$, $^{**}P < 0.01$, $^{***}P < 0.001$).

Isolation of in vivo LDL and modification of LDL and isolation of LDL⁻

Low density lipoprotein (LDL) was isolated from human plasma (USC blood bank) by density gradient ultra centrifugation and pooled from multiple expired plasma LDL donors as obtained from the USC blood bank (L-80 XP centrifuge, SW-41 rotor, Fullerton CA) [29]. LDL ($\delta = 1.019 - 1.063$) was then collected and washed with phosphate-buffered saline (PBS) several times using a Millipore (Bedford, MA) centrifugal filtering device with a 30 kDa cut-off. Anion exchange liquid chromatography using a stepwise sodium chloride gradient to isolate nLDL, LDL^{-}, and LDL^{2-} to analyze the percentage of LDL^{-}. HPLC was performed to analyze the percentage of LDL^{-}. Concentrated LDL (at 200 μg/ml) was then incubated with different concentrations of either $ONOO^{-}$ or SIN-1 for 30 min at 37 °C. Sin-1 was used as a donor of ·NO and $O_2{\cdot}^{-}$ to form $ONOO^{-}$ and to corroborate findings of $ONOO^{-}$-treated LDL [30]. The concentration of $ONOO^{-}$ stock was measured prior to the individual experiments using UV absorption spectra ($\lambda_{302nm} = 1.67\ mM^{-1}\ cm^{-1}$) according to the manufacturer's specification (Upstate, Lake Placid, NY).

Analysis of LDL modifications

Oxidation: LDL post-translational modifications were assessed in *in vivo* LDL subfractions (LDL) and *in vitro* $ONOO^{-}$/SIN1-treated LDL. Protein oxidation was determined by a decrease in biotin labeling to the oxidized cysteine residues. Biotin labeling was performed by incubating biotin with LDL for 1 h at 37 °C to label free unmodified cysteine residues. *Nitrotyrosine:* Two micrograms of $ONOO^{-}$-treated LDL and 10 μg of *in vivo* LDL subfractions were spotted on Millipore PVDF membranes. Two micrograms BSA nitrated with 1 mM $ONOO^{-}$ was used as a positive control. Dithionite was used to reduce nitro groups in the positive control in order to show that the binding was specific. *Dot blot analyse:* Dot blots were performed at a 1:3000 dilution in TBS-Tween for primary nitrotyrosine antibody and 1:10000 dilution for anti-mouse secondary antibody. Similar procedures were performed for 4 μg of biotin-labeled LDL with a monoclonal anti-biotin antibody (dilution at 1:10,000) and a secondary antibody (dilution at 1:10,000), (Sigma, St. Louis, MO). Dot Blots were analyzed using an ECL chemiluminescence kit (Pierce, Rockford, IL), and densitometry was performed using an NIH Scion Image Software (Scion Corp., Frederick, MD) and a product of the density and area determined. The product was also normalized to protein used for both nitrotyrosine and cysteine oxidation analysis. Total nitrotyrosine was quantified by LC/EIS/MS for $ONOO^{-}$-treated LDL samples. Western blot densities for $ONOO^{-}$-treated LDL were plotted against the quantified content of nitrotyrosine in the samples and this standard curve was used to determine the quantity of nitrotyrosine in both the *in vivo* LDL sub-fractions as well as the SIN-1 treated LDL by extrapolation of the curve. Comparison of nitrotyrosine quantities in the $ONOO^{-}$-treated LDL were comparable to the findings by Leeuwenburgh et al. after normalization to a 1 mg/ml solution [5].

Lipid peroxide measurements

Lipid peroxidation and cholesterol hydroperoxides was measured by the leucomethylene blue assay with *tert*-butyl-hydroperoxide as a standard. LMB cocktail consisted of a 0.05 M pH 5 potassium phosphate buffer with 1.4 g of Triton-X-100 and 5 mg of hemoglobin to 100 ml total volume. Five micrograms of LMB was diluted in 8 ml of dimethylformamide and 0.8 ml of LMB dimethylformamide cocktail was added to 10 ml of potassium phosphate buffer. Fifty micrograms of LDL were incubated with 150 μl of LMB cocktail for 1 h to a final volume of 200 μl in 96 well plates. Total tryptophan in apoB-100 was relatively small and any tryptophan hydroperoxides should only be minor contaminants The colorimetric assay was measured at 650 nm after 1 h incubation at room temperature with a leucomethylene blue cocktail mixture [3]. Molar concentrations of lipid peroxides were determined from a standard curve and total yield of LOOH determined as a ratio of μmol LOOH/g of LDL protein.

Analysis of specific sites of LDL protein nitration

LDL^{-} and nLDL were isolated from *in vivo* LDL by HPLC using a stepwise NaCl gradient as previously described [29]. For 100 μM $ONOO^{-}$-treated LDL, tLDL was analyzed for oxidative modifications. Liquid chromatography tandem mass spectrometry (LC-MS/MS) was performed using a ThermoFinnigan Surveyor MS-Pump with a BioBasic-18 100 × 0.18 mm reverse phase capillary column. The column was equilibrated for 5 min at 1.5 μl/min with 95% solution A and 95% solution B (A, 0.1% formic acid in water; B, 0.1% formic acid in acetonitrile) and linear gradient was initiated 5 min after sample injection with a ramp to from 95% A to 35% A and 65% B after 50 min and 20% A and 80% B after 60 min. Analysis was obtained by the ThermoFinnigan LCQ Deca XP Plus ion trap mass spectrometer, equipped with a nanospray ion source (ThermoFinnigan) that employed a 4.5 cm metal needle (Hamilton, 950-00954), in a data-dependent acquisition mode. Electrical contact and voltage application to the probe tip were established via the nanoprobe assembly. Spray voltage was set at 2.9 kV and heated capillary temperature at 190 °C. Mass spectra were ac-

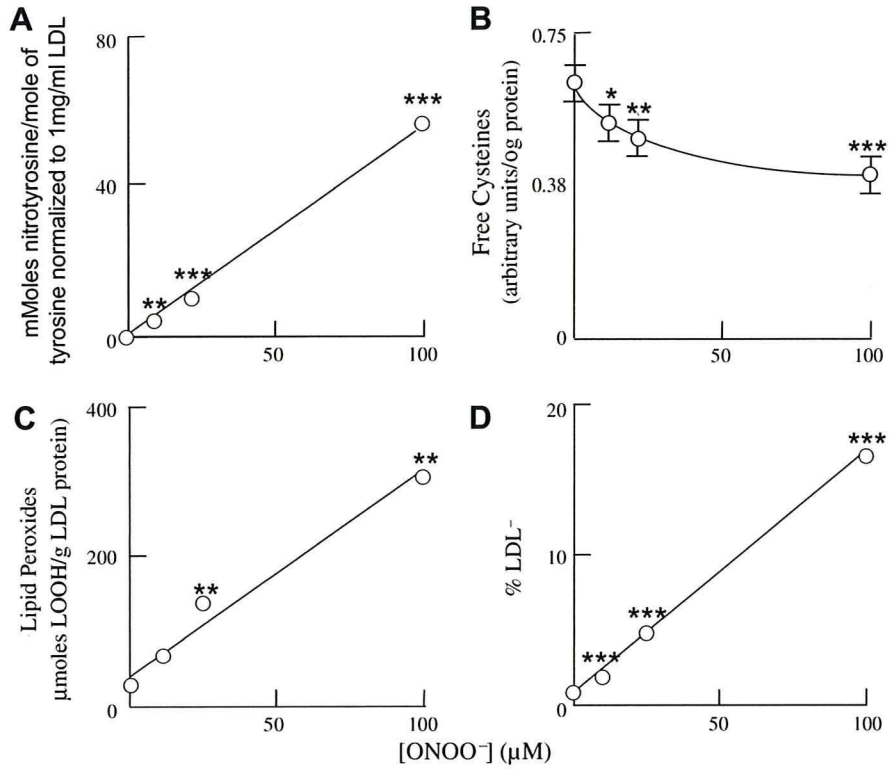

Fig. 3. $ONOO^-$-modified LDL. LDL samples were supplemented with different amounts of $ONOO^-$ and analyzed for (A) nitrotyrosine, (B) free cysteine (after biotin labeling), (C), lipid peroxides, and LDL^- content (percentage). ($n = 3$, $^*P < 0.05$, $^{**}P < 0.01$, $^{***}P < 0.001$).

Table 2
LC/MS/MS analyses of $ONOO^-$-modified LDL Apo-B100

Secondary structure	Peptide	Modified AA	Sequence	MSc	charge	XC	Δcn	Modification	% modified
α_1	101–110	NO_2-Tyr^{103}	EVY[a]GFNPEGK	29	1	1.7	0.4	Nitrotyrosine	49.9 ± 1.7
α_1	401–427	NO_2-Tyr^{413}	VHANPLLIDWTY[a]LVALIPEPSAQQLR	33	2	2.6	0.3	Nitrotyrosine	53.7 ± 1.4
α_1	655–669	NO_2-Tyr^{666}	IEGNLIFDPNNY[a]LPK	28	2	2.8	0.4	Nitrotyrosine	81.5 ± 3.3
α_2	2523–2534	NO_2-Tyr^{2524}	MY[a]QMDIQQELQR	65	2	3.7	0.4	Nitrotyrosine	66.6 ± 5.9
β_2	3481–3497	NO_2-Tyr^{3489}	LSLESLTSY[a]FSIESSTK	20	2	0.2	2.0	Nitrotyrosine	41.3 ± 0.6
β_2	3767–3772	NO_2-Tyr^{3771}	EIQJY[a]K	25	1	0.1	1.3	Nitrotyrosine	29.1 ± 0.7
β_2	3953–3973	HO-Phe^{3965}	DFSAEYEEDGKFEGLQEWEGK	30	2	3.7	0.4	HO-phenylalanine	86.3 ± 0.2
α_3	4088–4098	NO_2-Tyr^{4088}	Y[a]HWEHTGLTLR	28	2	2.1	0.3	Nitrotyrosine	95.3 ± 0.8
			Quantification of NO_2-Y mmol NO_2-Y/(mol Y) 54.2 ± 1.3						

[a] Full annotated MS spectra are represented in the order presented in this table in Figs. 13–20 of the Supplemental section.

quired at 400–2000 *m/z* using a Top five method where the five most intense ions for the full scan were subjected to collision induced dissociation, using helium (ms/ms). Peptide identification was achieved using Mascot 1.9 search software (Matrix Science) with confirmatory or complementary analyses by TurboSequest as implemented in the Bioworks Browser 3.2, build 41 (Thermo-Finnigan). Spectra were searched against the NCBI human genome database, NCBI build 35. Aromatic nitration and hydroxylation as well cysteine oxidation were assessed using Mascot 1.9 (Matrix Science) for cysteic acid, nitrotyrosine and nitrotryptophan, with confirmatory or complementary analyses that employed TurboSequest as implemented in the Bioworks Browser 3.2, build 41 (ThermoFinnigan) [31,32]. In addition to cysteic acid (+48 Da), nitrotyrosine (+45 Da) and nitrotryptophan (+45 Da), Sequest was used to assess the presence of single or doubly oxidized cysteine (+16 and +32, respectively) as well as tryptophan with both a nitration and oxidation (+61). Quantification of nitrated peptides was carried out by analysis of peak nitration to peak unmodified plus peak modified peptides (NO_2-peptide/(NO_2-peptide + unmodified peptide). Further positive peptides were analyzed against their y- and b-ions to insure that peptides measured were present and not false positives. They were further analyzed against their peak height to noise ratio.

Circular dichroism spectral analysis of protein structure

Circular dichroism (CD) allows for probing the secondary structure content of proteins. The CD spectrum of modified LDL provides a means to determine the conformational changes of secondary structure in apoB-100 (α-helix, anti-parallel and parallel β-sheet, β-turn, and random coil). *In vivo* isolated LDL and 100 μM $ONOO^-$-treated LDL sub-fractions of LDL isolated from HPLC were concentrated and dialyzed to a 0.1 mg/ml solution in chloride free phosphate buffer saline for CD analysis. CD spectra were measured at least ten times to determine the protein structure. Different secondary structures are represented by the spectrum between 200 and 260 nm. Deconvolution analysis using CD spectra software (CDNN) allowed for assessment of the percent structural integrity in the LDL sub-fractions of modified LDL.

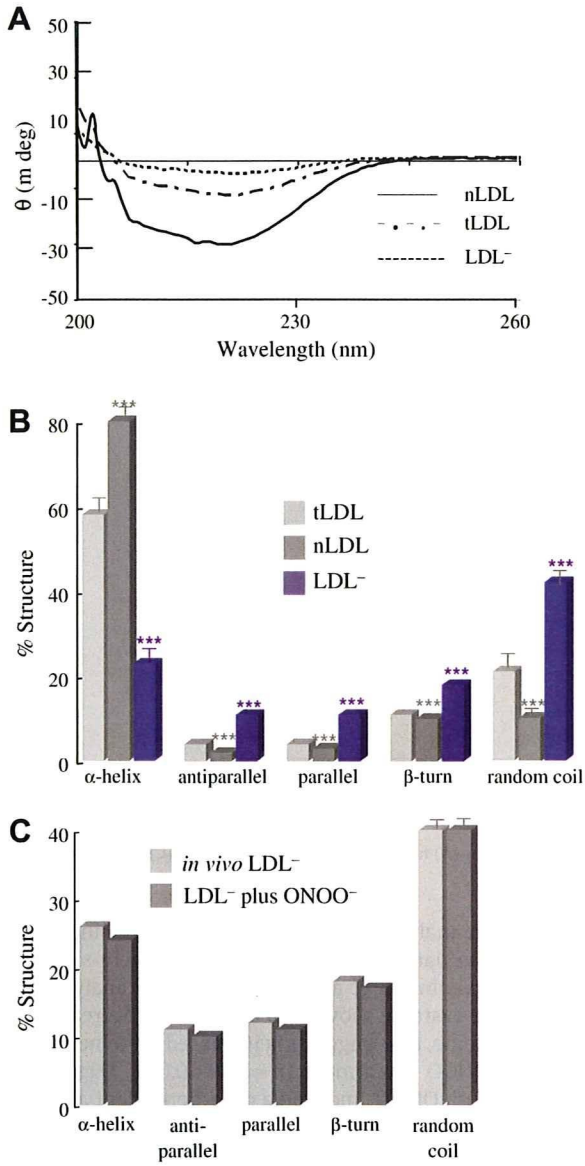

Fig. 4. Circular dichroism spectral analyses of $ONOO^-$-modified LDL. tLDL was treated with 10 μM $ONOO^-$ as described in Materials and methods); the $ONOO^-$-treated tLDL was fractionated into nLDL and LDL^- components and CD spectra were determined. (A) Circular dichroism spectra of LDL sub-fractions. (B) Secondary structure of different LDL sub-fractions. CD deconvolution software wasused to determine the changes in the structures of the LDL sub-fractions. (C) Comparison of secondary structure components in *in vivo* LDL^- and LDL^- from $ONOO^-$-treated tLDL. Data taken from Fig. 2B (for *in vivo* LDL^-) and Fig. 4B (LDL^- fraction of the $ONOO^-$-treated tLDL). ($n = 3$, $^*P < 0.05$, $^{**}P < 0.01$, $^{***}P < 0.001$).

Endothelial cell culture

Bovine aortic endothelial cells (BAEC) between passages five and nine were grown to confluent monolayers in high glucose (4.5 g/l) DMEM (Dulbecco's Modified Eagle's Medium) supplemented with 10% heat-inactivated fetal bovine serum (Gemcell, West Sacramento, CA) and 100 U/ml penicillin–streptomycin (Irvine Scientific, Santa Ana, CA), for 48 h in 5% CO_2 at 37 °C.

Binding and uptake of LDL particles

Control and 100 μM $ONOO^-$-supplemented LDL particles were treated with 75 mg/ml DiI overnight. DiI-labeled LDL particles were ultracentrifuged, collected, dialyzed, and sterilized to remove the DiI particulate [33]. BAEC were treated with 10 μg/ml DiI-labeled LDL at 0 °C for 90 min or at 37 °C for 4 h for LDL binding or uptake experiments, respectively [33]. Cells were also treated with10 μg/ml DiI-labeled LDL with 200 μg/ml of excess unlabeled LDL as a control to exclude DiI labeling of cell membranes and for LDL binding and uptake specificity [33]. Cells were washed thoroughly with DMEM three times after treatment, washed in PBS three times, fixed in paraformaldehyde for 10 min at room temperature, and washed six more times with PBS. Cells were mounted in DAPI-containing mounting medium and visualized using an Axiom 200 M Zeiss Fluorescent Microscope (Zeiss, Thornwood, NY) was performed using a DAPI filter for the nucleus and CY3 filter for the DiI-labeled LDL. Quantification of mean intensity and image analysis were assessed by slidebook software (Santa Monica, CA).

Receptor blocking

BAEC were pre-treated for 1 h with a 1:250 dilution of receptor blocking antibodies to LOX-1, CD36, SR-A, and LDL-R to determine receptor involvement in control- and $ONOO^-$-LDL binding and uptake. BAEC were pre-treated with receptor blocking antibodies as follows: (1) no receptor blocking (all active), (2) All receptors blocked (all four inactive), (3) all receptor blocking except LOX-1 (LOX-1 active), (4) all receptor blocking except CD36 (active CD36), (5) all receptor blocking except SR-A (Active SR-A), and (6) all receptor blocking except LDL-R (active LDL-R). Uptake and binding of DiI-labeled control- and $ONOO^-$-LDL were performed by the methods described above.

Statistical analysis

Data were expressed as mean ± SD and compared among separate experiments ($n = 3$). For comparisons between two groups, two-sample independent-group *t*-tests were used (one tail and type three *t*-test analysis). Comparisons of multiple values were made by one-way analysis of variance (ANOVA), and statistical significance among multiple groups determined by the Tukey test (for pair-wise comparisons of means between control and treatments). *P*-values of <0.05 are considered statistically significant.

Results

Post-translational modifications of in vivo LDL^-

In vivo native LDL (nLDL) and LDL^- were isolated from total-LDL (tLDL) using anion exchange chromatography as described in Materials and methods. The average of LDL^- isolated from tLDL *in vivo* was 1.05 ± 0.05% of the total-LDL protein for the purposes of these experiments. LDL nitration was assessed by immunoreactivity to nitrotyrosine antibody (Fig. 1A). While nitrotyrosine was not detectable in either nLDL or tLDL, it was prominent in the LDL^- fraction ($n = 3$; $P < 0.001$; Fig. 1A). Oxidation of the nine free cysteine residues in the *in vivo* LDL sub-fractions was assessed by biotin labeling of free cysteine (Fig. 1B). LDL^- harbored a significantly lower level of free cysteine in comparison with nLDL and tLDL: nLDL < tLDL < LDL^-) ($n = 3$, $P < 0.001$), thus suggesting an elevated amount of cysteine oxidation in LDL^- (Fig. 1B). Also worth noting was a threefold increase in lipid peroxides in LDL^- in comparison with nLDL and tLDL ($n = 3$, $P < 0.001$) (Fig. 1C).

LC/MS/MS analyses of *in vivo* LDL-revealed specific modifications in the apoB-100 moiety (Table 1): tyrosine (Tyr), tryptophan (Trp), cysteine (Cys), and phenylalanine (Phe) underwent nitration/oxidation in both α helices and β-sheets; namely, α_1 ($Tyr^{276,666,720}$, Trp^{583}), α_2 (Tyr^{2523}), β_2/α_3(Phe^{3969}), β_1 (Cys^{1112}), α_3 (Tyr^{4141}), and β_2 ($Tyr^{3139,3295,3489}$) (Table 1) as corroborated by the Mascot and

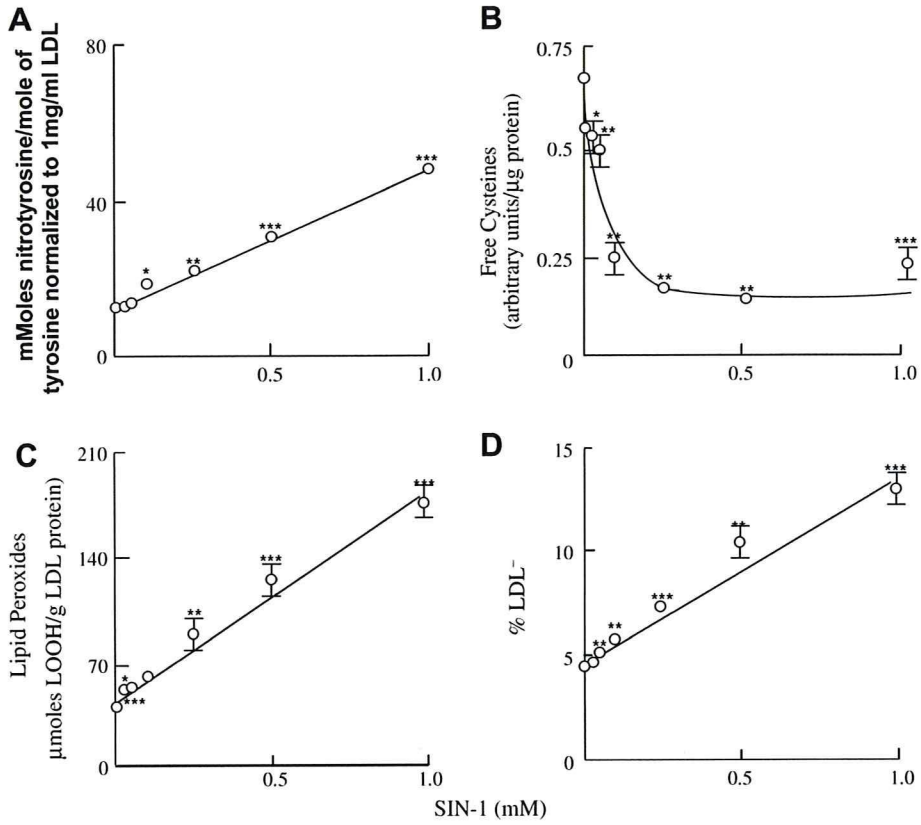

Fig. 5. SIN-1-modified LDL. LDL particles were incubated with different amounts of SIN-1 and analyzed for (A) nitrotyrosine, (B) free cysteine, (C) lipid peroxides, and (D) percentage of LDL⁻ as described in Materials and methods section. ($n = 3$, $^{*}P < 0.05$, $^{**}P < 0.01$, $^{***}P < 0.001$).

Sequest scores as well as analysis of peptide and peptide ions masses. These data suggested a large extent of protein modification in the electronegative subfraction or modified LDL subfraction *in vivo* which are consistent with a purification of the *in vivo* oxLDL (LDL⁻). It was further noted that the nitration levels were similar in content to that of 100 µM $ONOO^-$-treated LDL. Cys^{1112} in β_1 sheet was oxidized to cysteic acid. Modifications of these peptides are shown in the supplemental (Supplemental Figs. 1–12) and indicate that spectra are accurate.

Circular dichroism and protein post-translational modifications

Previous studies have suggested that LDL⁻ had significantly unfolded α-helical structure [11,34]. Circular dichroism analysis was used in order to establish an association between specific LDL protein modifications and protein structure [3,11,34]. *In vivo* LDL subfractions (Fig. 2A, B) displayed a decrease in optical rotativity at 200–260 nm from LDL⁻ to tLDL to nLDL (Fig. 2A). Increasing optical rotativity at the 220 nm valley reflects a loss in α-helical character and an increase in β-structural components as determined by deconvolution (Fig. 2B). Deconvolution analysis using CD spectra software (CDNN) determined the percent structural integrity of the aforementioned components in LDL sub-fractions of *in vivo* modified LDL. The α-helical content in nLDL (~90%) was largely higher than that in LDL⁻ (~25%), thus suggesting substantial protein unfolding in the latter. These data suggest an association between α-helical nitration (Table 1), lipid peroxidation (Fig. 1C), and protein unfolding (Fig. 2) in LDL⁻.

Characteristics of $ONOO^-$-modified LDL

Treatment of LDL with $ONOO^-$ induced tyrosine nitration in apoB-100 protein in a dose-dependent manner (Fig. 3A; $n = 3$; $P < 0.01$). Upon analysis of total mmol of nitrotyrosine to tyrosine precursor, these data for $ONOO^-$-treated LDL were similar to the work by Leeuwenburgh et al. [5]. Densitometry analysis of biotin labeling of free cysteine showed an exponential decrease in the level of free cysteine, thus suggesting increased cysteine oxidation in response to $ONOO^-$ treatment ($n = 3$, $P < 0.001$) (Fig. 3B). Treatment of LDL with $ONOO^-$ induced a dose-dependent accumulation of lipid peroxides in LDL (Fig. 3C). HPLC analysis revealed a dose-dependent linear increase in the percentage of LDL⁻ in response to $ONOO^-$ treatment (Fig. 3D); this increase was paralleled by an increase in nitrotyrosine- (Fig. 3A) and lipid peroxide (Fig. 3C) content. Oxidized lipid-derived aldehydes were also significantly elevated in response to $ONOO^-$ treatment (data not shown). It may be surmised that both lipid peroxides and nitrotyrosine formation are involved in $ONOO^-$-induced modification of LDL to an atherogenic form (LDL⁻).

Table 2 lists the nitration and oxidation sites in the apoB-100 protein upon treatment with 100 µM $ONOO^-$: $\alpha_1(Tyr^{103,413,666})$, α_2 (Tyr^{2524}), β_2 ($Tyr^{3490,3791}$), β_2/α_3 (Phe^{3965}), and α_3 (Tyr^{4088}). Neither *in vivo* LDL⁻ (Table 1) nor $ONOO^-$-treated LDL (Table 2) showed nitration of β_1. Similarly to *in vivo* LDL⁻, $ONOO^-$ treatment elicited β_2 nitration at Tyr^{3490} (in addition to Tyr^{3791}). The phenylalanine residue between β_2 and α_3 underwent hydroxylation as also observed in *in vivo* LDL⁻. These data strengthen the notion that *in vivo* LDL⁻ may originate from $ONOO^-$-driven modifications at specific sites in apoB-100 protein. Modifications of the peptides shown above are described in the supplemental (Supplemental Figs. 13–20).

Circular dichroism analysis of $ONOO^-$-treated LDL

$ONOO^-$-treated LDL (Fig. 4A) displayed a decrease in optical rotativity at 200–260 nm for LDL⁻ as compared to nLDL. There was a

distinctive difference in the CD spectra for LDL sub-fractions at 220 nm (LDL^- > tLDL > nLDL). As mentioned above, increasing optical rotativity at 220 nm reflects a loss in α-helical structure and an increase in β-sheet structure that was confirmed by CD deconvolution software (CDNN) assessing the percent structural integrity of the different LDL sub-fractions components of $ONOO^-$-modified LDL (Fig. 4B). Interestingly, the percentage of structural components in *in vivo* LDL^- and that of $ONOO^-$-treated LDL were similar (Fig. 4C).

SIN-1-modified LDL

Because atherosclerotic lesions have increased activities of iNOS/eNOS and NADPH oxidase, a flux of ·NO and $O_2^{\cdot -}$ (to yield $ONOO^-$) may be mimicked by SIN-1 and may further support findings by our laboratory showing increased nitration at bifurcations where oscillatory flow occurs and where atherosclerosis is prone to develop [15]. Nitrotyrosine- (Fig. 5A) and lipid peroxide (Fig. 5C) accumulation as well as the percentage of LDL^- formation (Fig. 5D) following incubation of LDL with SIN-1 were similar to those observed with $ONOO^-$ (Fig. 3). SIN-1 also induced an oxidation of cysteine residues (Fig. 5B) greater than that obtained with $ONOO^-$ (Fig. 3B).

Binding and uptake of $ONOO^-$-modified LDL

The biological significance of modified LDL was assessed with respect to LDL binding to- (Fig. 6) and uptake by (Fig. 7) bovine aortic vascular endothelial (BAEC) cells. Binding experiments, performed at 0 °C, are shown for DiI-labeled LDL (Fig. 6A) and DiI-

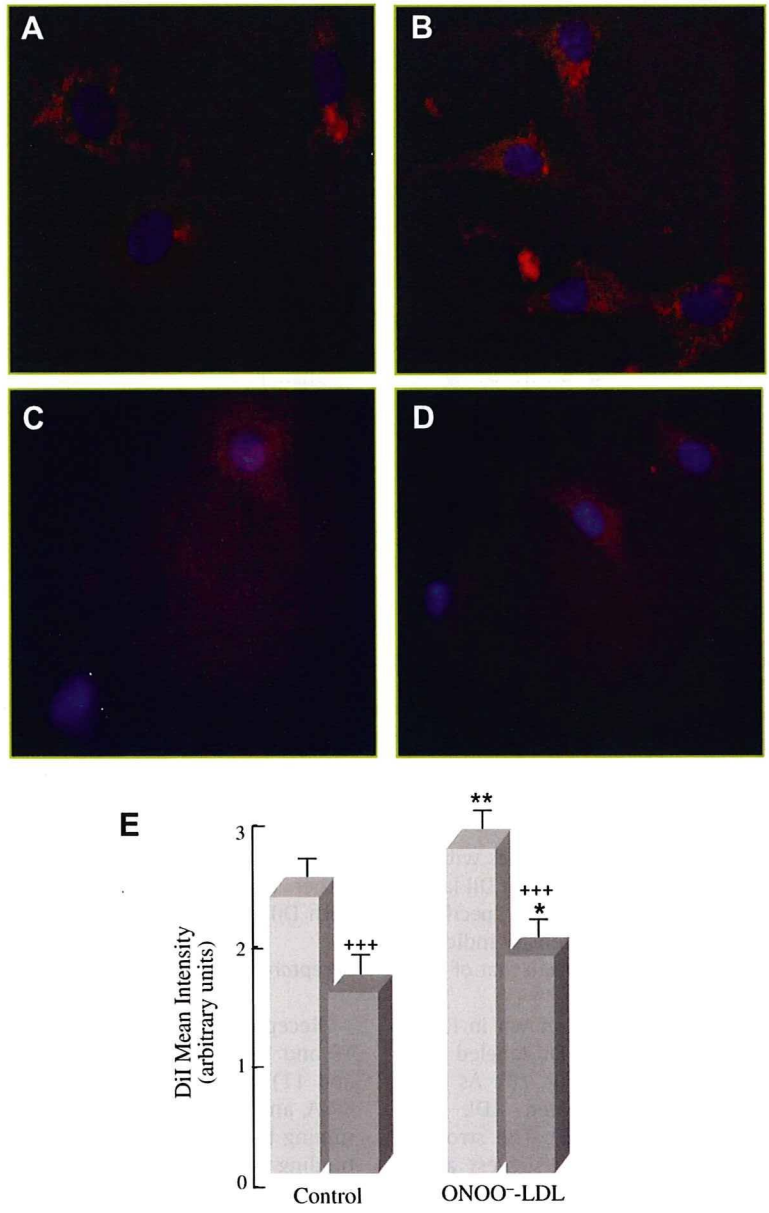

Fig. 6. Binding of $ONOO^-$-modified LDL. LDL binding experiments were performed at 0 °C for 90 min with the following conditions: (A) control-LDL 10 μg/ml DiI-LDL, (B) $ONOO^-$-treated LDL 10 μg/ml DiI-PN-LDL, (C) control-LDL 10 μg/ml DiI-LDL + 200 μg/ml unlabeled control-LDL, and (D) $ONOO^-$-treated LDL 10 μg/ml DiI-PN-LDL + excess unlabeled $ONOO^-$-treated LDL 200 μg/ml. Binding mean intensity of DiI-labeled LDL was quantified using Axiom 200 M Zeiss Fluorescent Microscope (E). Experiments were performed in triplicate and statistical significance to control-LDL and to the excess unlabeled LDL ($P < 0.01$) was determined. ($n = 3$, $^{+,*}P < 0.05$, $^{++,**}P < 0.01$, $^{+++,***}P < 0.001$).

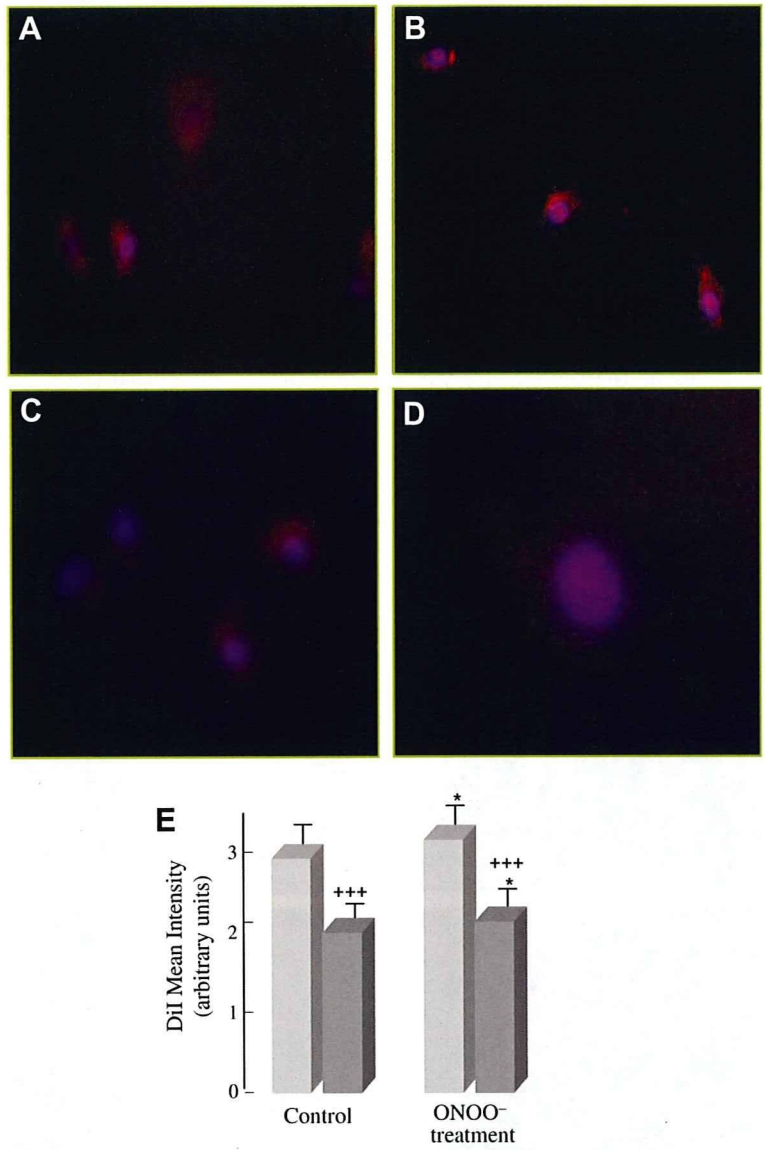

Fig. 7. Uptake of $ONOO^-$-modified LDL. LDL uptake experiments were performed at 37 °C for 4 h with the following conditions; (A) control-LDL 10 μg/ml DiI-LDL, (B) $ONOO^-$-treated LDL 10 μg/ml DiI-PN-LDL, (C) control-LDL 10 μg/ml DiI-LDL + 200 μg/ml unlabeled control-LDL, and (D) $ONOO^-$-treated LDL 10 μg/ml DiI-PN-LDL + excess unlabeled $ONOO^-$-treated LDL 200 μg/ml (D). Uptake mean intensity of DiI-labeled LDL was quantified using Axiom 200 M Zeiss Fluorescent Microscope (E). Experiments were performed in triplicate and statistical significance to control-LDL (*) and to the excess unlabeled LDL (*) was determined. ($n = 3$, $^{+,*}P < 0.05$, $^{++,**}P < 0.01$, $^{+++,***}P < 0.001$).

labeled, $ONOO^-$-treated LDL (Fig. 6B). Similar approaches with an excess of 200 μg/ml unlabeled LDL were used to rule out DiI labeling of cell membranes and ascertain LDL binding specificity (Fig. 6C, D). Analysis of the mean fluorescence intensity indicated that binding of $ONOO^-$-treated LDL was stronger than that of control LDL (Fig. 6E).

Uptake experiments, performed at 37 °C, are shown in Fig. 7 with a similar approach to that in Fig. 6: DiI-labeled LDL (Fig. 7A) and DiI-labeled, $ONOO^-$-treated LDL (Fig. 7B). As with binding experiments, uptake of $ONOO^-$-treated LDL was slightly higher than that of native LDL (Fig. 7E). The stronger binding and uptake of $ONOO^-$-treated LDL may suggest alternate uptake mechanisms as well as an increased uptake of unfolded proteins.

In the presence of a 20-fold excess of native LDL (Figs. 6C and 7C) or $ONOO^-$-treated LDL (Figs. 6D and 7D), respectively, binding and uptake were significantly inhibited (Figs. 6E and 7E), thus suggesting that LDL is binding to- and taken up by cells rather than nonspecific labeling of BAEC plasma membranes with DiI.

Receptor-dependent binding and uptake of control- and $ONOO^-$-LDL

Receptor-dependent binding (Figs. 8 and 9) and uptake (Figs. 10 and 11) of control- (Figs. 8 and 10) and $ONOO^-$-LDL (Figs. 9 and 11) was determined by receptor blocking of LOX-1, CD36, SR-A, and LDL-R with receptor blocking antibodies and by determining the amount of DiI-control-LDL and DiI-$ONOO^-$-LDL mean binding and uptake intensities. Analysis of control-LDL showed that the majority of the control lipoprotein binding was initiated by LDL-R (Fig. 8E, G, $P < 0.01$); however there were minimal binding differences between all receptors blocked in the presence of active LOX-1 (Fig. 8B, G), CD36 (Fig. 8C, G), and SR-A (Fig. 8D, G). However, LDL-R was not completely involved in

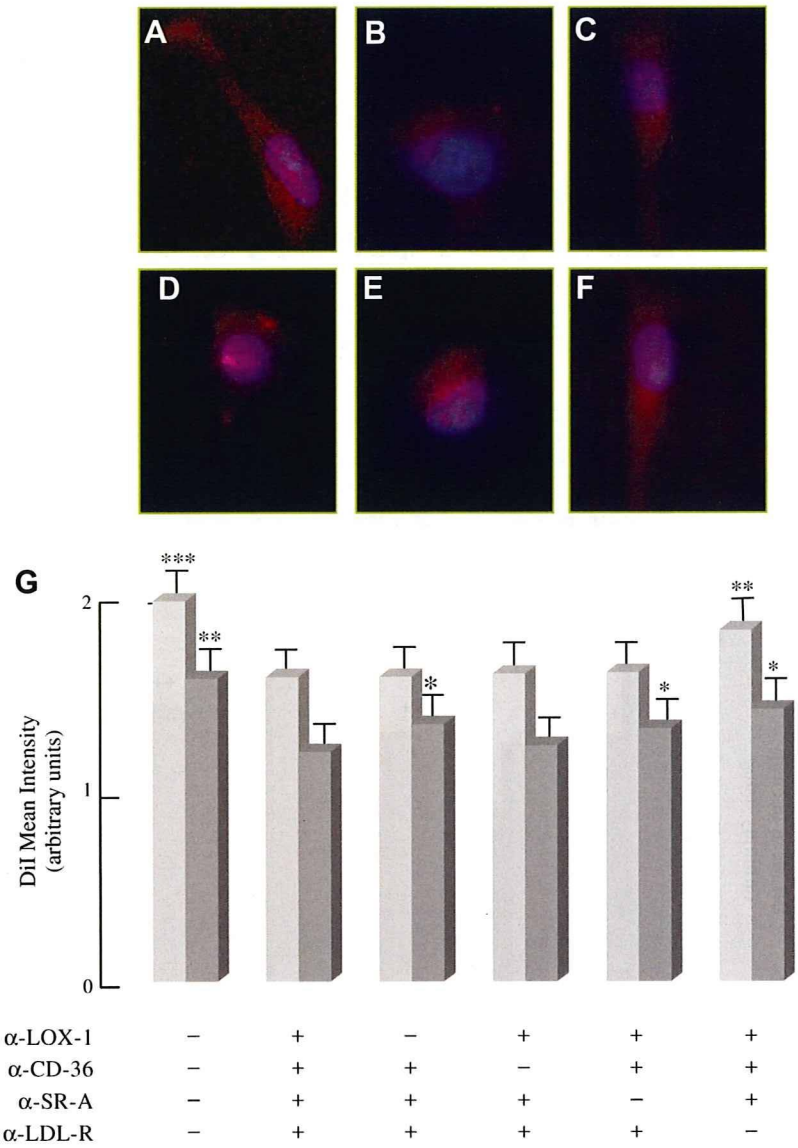

Fig. 8. Binding of control-LDL after receptor blocking. LDL receptor blocking was performed for 1 h at 37 °C and binding was determined at 0 °C with 10 μg/ml DiI-control-LDL and 10 μg/ml DiI-control-LDL with 200 μg/ml excess unlabeled LDL for 90 min by the following conditions; (A) no receptor blocking with 10 μg/ml DiI-control-LDL, (B) all four receptor's blocked with 10 μg/ml DiI-control-LDL (C) active LOX-1, (D) active CD36 with 10 μg/ml DiI-control-LDL, (E) active SR-A with 10 μg/ml DiI-control-LDL, and (F) active LDL-R with 10 μg/ml DiI-control-LDL. Binding mean intensity of DiI-control-LDL was quantified using Axiom 200 M Zeiss Fluorescent Microscope (G). Images are not shown for excess unlabeled control-LDL but intensities were quantified. Experiments were performed in triplicate and statistical significance was determined to all receptors blocked to determine receptors significantly involved in the binding of DiI-labeled control-LDL ($n = 3$, $^{*}P < 0.05$, $^{**}P < 0.01$, $^{***}P < 0.001$). –10 mg/ml DiI-labeled control-LDL –10 mg/ml DiI-labeled control-LDL + 200 mg/ml excess unlabeled control-LDL.

the binding of control-LDL since active LDL-R was unable to completely restore binding to no receptor blocking (Fig. 8A, G). Incubating cells with excess unlabeled LDL was able to reduce the binding intensity of DiI-LDL suggesting that DiI was only minimally labeling the membranes and was not the majority of the labeling. These findings also demonstrate that control-LDL is bound to the non-atherogenic LDL-R with minimal binding from the three oxLDL-R, thus suggesting that the small amount of oxLDL *in vivo* may be binding to scavenger receptors *in vitro*.

$ONOO^-$-modified LDL was significantly bound by LOX-1 (Fig. 9C, G, $P < 0.05$), CD36 (Fig. 9D, G, $P < 0.001$) and SR-A (Fig. 9E, G, $P < 0.01$) with SR-A and CD36 having the largest impact on binding whereas active LDL-R had no impact on LDL binding (Fig. 9F, G). These findings suggest that $ONOO^-$-treated LDL is not binding through an aggregated-LDL-R-dependent mechanism but rather by each of the three scavenger receptors (LOX-1, CD36, and SR-A).

Receptor-dependent uptake of control-LDL (Fig. 10) demonstrated that the particle is taken up significantly by LDL-R (Fig. 10F, G $P < 0.001$), whereas there is minimal involvement with LOX-1 (Fig. 10C, G), CD36 (Fig. 10D, G) and SR-A (Fig. 10E, G) scavenger receptors. These findings further support the motion that control-LDL has minimal modified LDL and is minimally atherogenic as compared to $ONOO^-$-LDL.

The receptor-dependent uptake of $ONOO^-$-treated LDL was significantly elevated for LOX-1 (Fig. 11C, G, $P < 0.05$), CD36 (Fig. 11D, G, $P < 0.01$), SR-A (Fig. 11E, G, $P < 0.001$), whereas LDL-R (Fig. 11F, G) was not significantly different from all receptors blocked suggesting that $ONOO^-$-LDL is not internal-